Dubna, August 7 - 17, 2006

Three-body decay of nuclear resonances

A.S. Jensen[1], D.V.Fedorov[1], E. Garrido[2], H. Fynbo[1], R. Alvarez-Rodriguez[1]

[1]IFA, University of Aarhus, DK-8000 Aarhus C

[2]Instituto de Estructura de la Materia, CSIC, E-28006 Madrid

CONTENT

Theoretical formulation:

Coordinates: $(\boldsymbol{x}, \boldsymbol{y})$ are mass scaled Jacobi coordinates

$\boldsymbol{r_{ij}}$ is the vector connecting particle i and j

$$x^2 = r_{ik}^2 \ \ \frac{m_i m_k}{m(m_i+m_k)}$$

$$y^2 = r_{j,ik}^2 \ \ \frac{m_j(m_i+m_k)}{m(m_i+m_k+m_j)}$$

$$\rho^2 = x^2 + y^2 = \frac{1}{m(m_i+m_k+m_j)} \ \ \Sigma_{i<j}\, m_i m_j r_{ij}^2$$

$\Omega = \{\Omega_x, \Omega_y, \alpha\}$, i.e. directions of $(\boldsymbol{x}, \boldsymbol{y})$ and $\tan\alpha = \frac{x}{y}$

Complex scaling: $\rho \rightarrow \rho \exp(i\theta)$

Adiabatic hyperspherical expansion:

Choose interactions and solve Faddeev equations for each ρ

Compute angular eigenvalues λ_n and eigenfunctions $\{\Phi_n(\rho, \Omega)\}$

The three-body bound state or resonance wave function Ψ is:

$$\begin{aligned}\Psi(\boldsymbol{x}, \boldsymbol{y}) &= \Sigma_n\, f_n(\rho)\Phi_n(\rho, \Omega) \\ &= \Sigma_n\, f_n(\rho)\Big(\phi_1^{(n)}(\rho, \Omega) + \phi_2^{(n)}(\rho, \Omega) + \phi_3^{(n)}(\rho, \Omega)\Big)\end{aligned}$$

Solve radial equations: $f_n(\rho)$ and complex energy eigenvalues

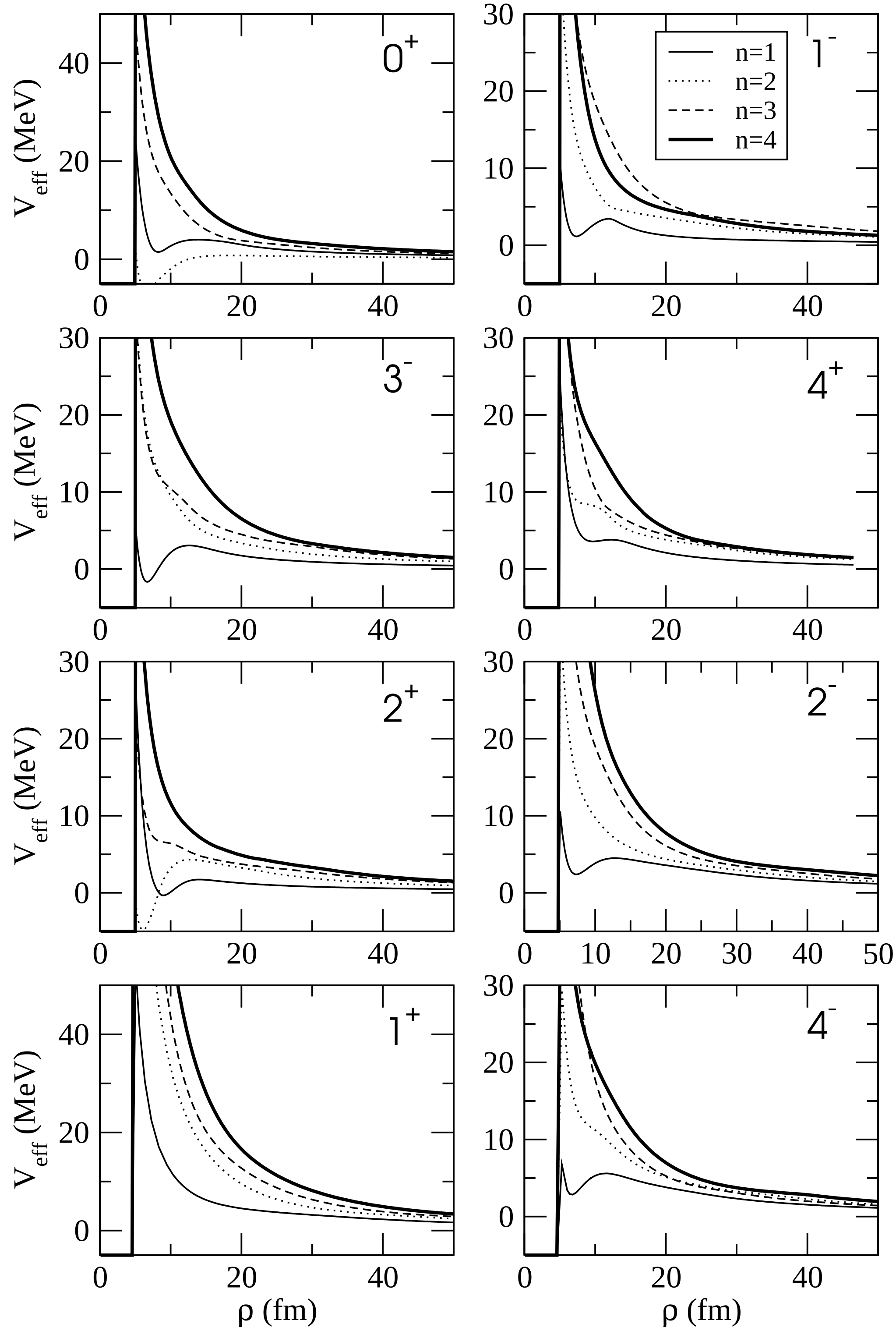

Figure 1: The real parts of the four lowest adiabatic effective potentials as functions of ρ for the ^{12}C resonances with J^{π} as indicated on the figure.

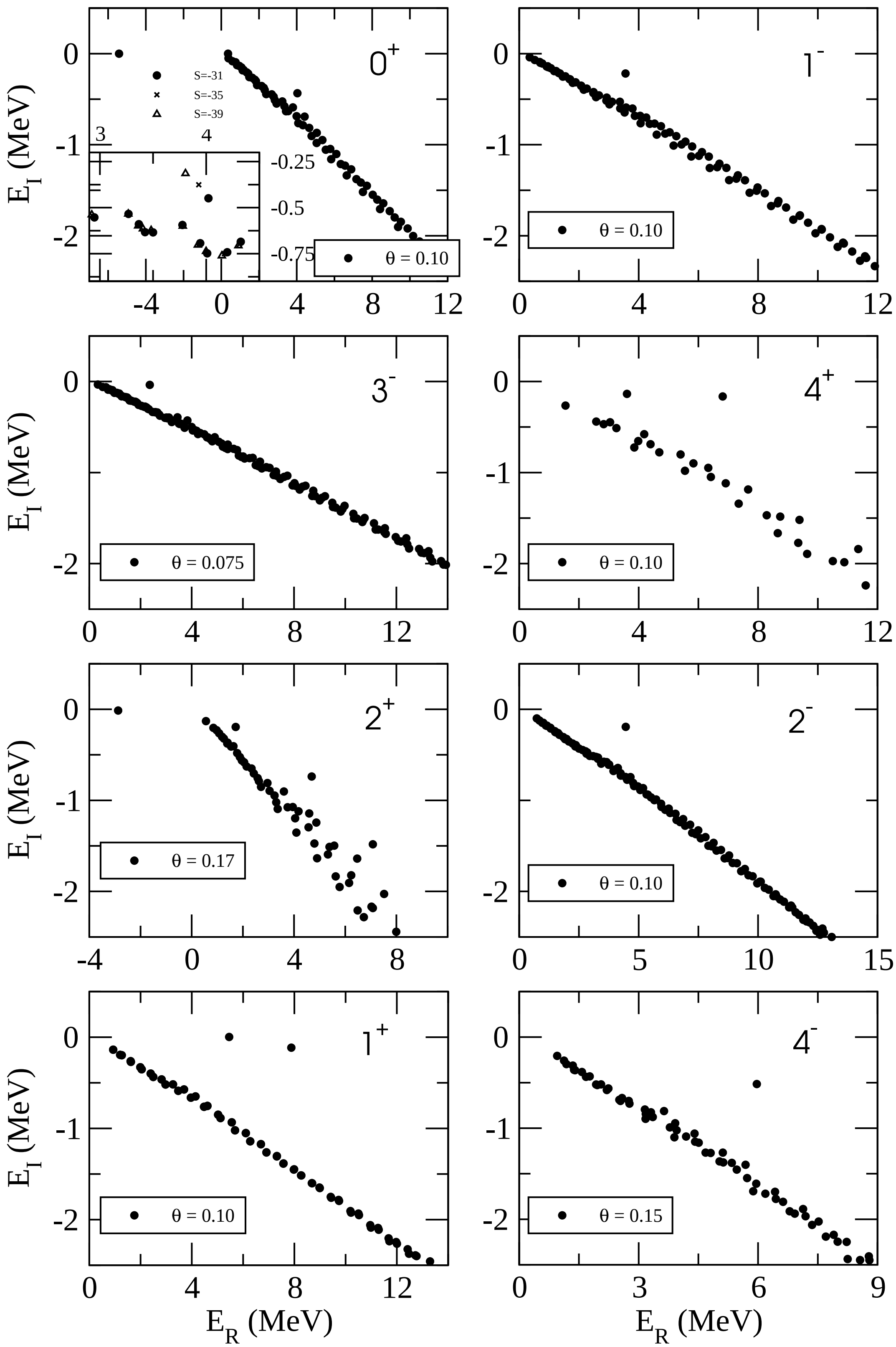

Figure 2: The real and imaginary parts of the ^{12}C resonances after rotation by the angle θ.

Table 1. J^π; $E_{R,exp}$ (MeV); $\Gamma_{R,exp}$ (keV); $E_{R,th}$ (MeV); $\Gamma_{R,th}$ (keV); 3-body potential parameters: S (MeV); b (fm); rotation angle (rad).

J^π	$E_{R,exp}$	$\Gamma_{R,exp}$	$E_{R,th}$	$\Gamma_{R,th}$	S	b	θ
0^+	-7.25	bound	-6.113	bound	-39	5	0.0005
	0.38	8.5×10^{-3}	0.318	5.97×10^{-3}	-39	5	0.0005
			4.037	0.922	-31	5	0.1
1^-	3.57	315	3.569	432.8	-6.8	5	0.1
3^-	2.37	34	2.363	71.6	-1.7	5	0.075
4^+	6.81	258	6.808	361.3	-26	5	0.1
			3.633	300.0	-26	5	0.1
2^+	-2.875	bound	-2.875	bound	-21.5	5	0.17
	3.88	430	1.730	387.7	-21.5	5	0.17
			4.690	1.459	-21.5	5	0.17
			7.057	3.051	-21.5	5	0.17
2^-	4.55	260	4.464	464.1	-7.3	5	0.1
	6.08	375					
1^+	5.43	18.1	–	–	-154.5	5	
	7.84	43.6	–	–	-141.5	5	

Figure 3: Experimental and computed energies and widths of ^{12}C resonances with J^π.

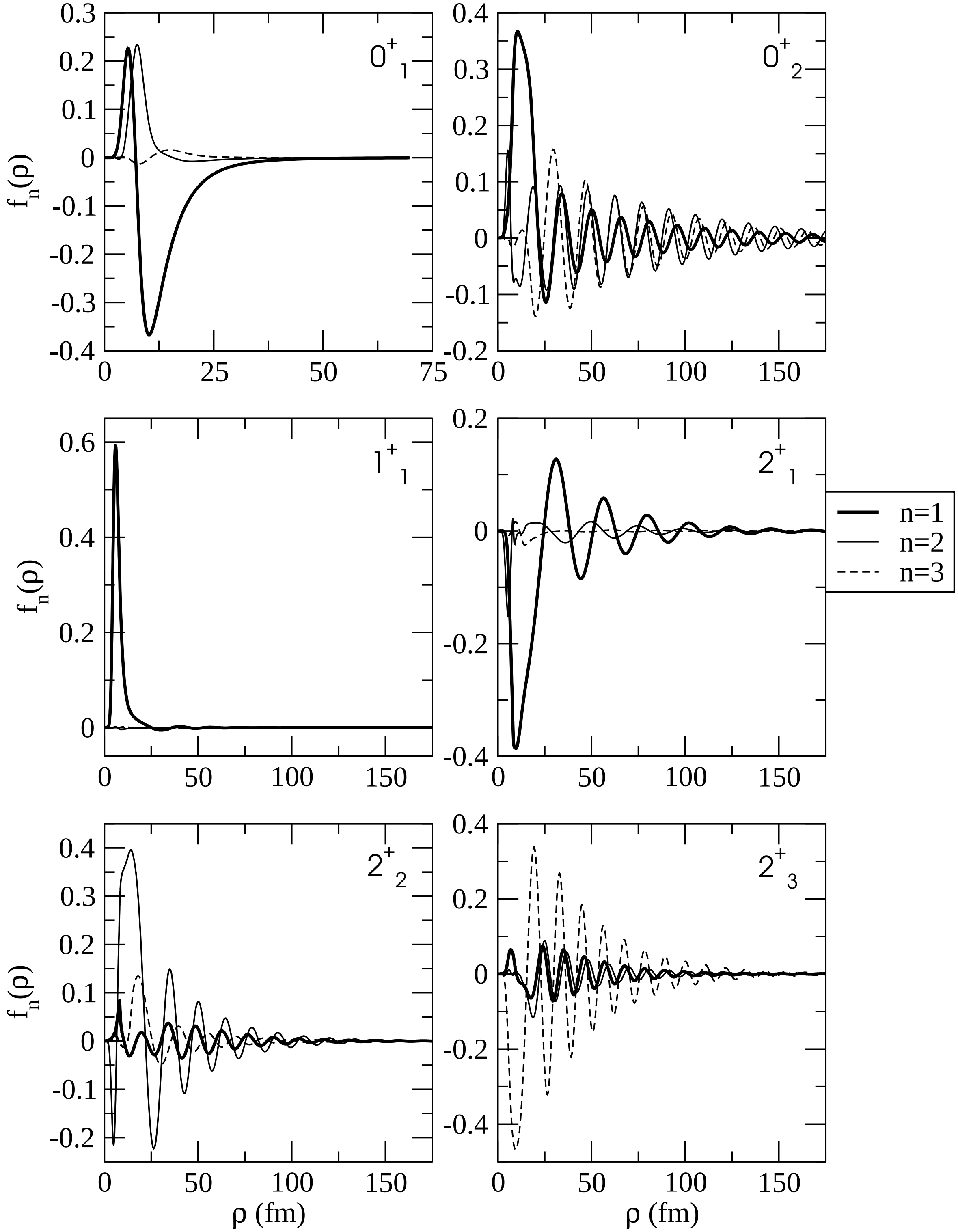

Figure 4: The real parts of the three lowest adiabatic radial wavefunctions as functions of ρ for the ^{12}C resonances with J^{π}.

$\Psi(\boldsymbol{x}, \boldsymbol{y}) = \Sigma_n \, f_n(\rho)\Phi_n(\rho, \Omega)$

Each fall off exponentially while oscillating around zero

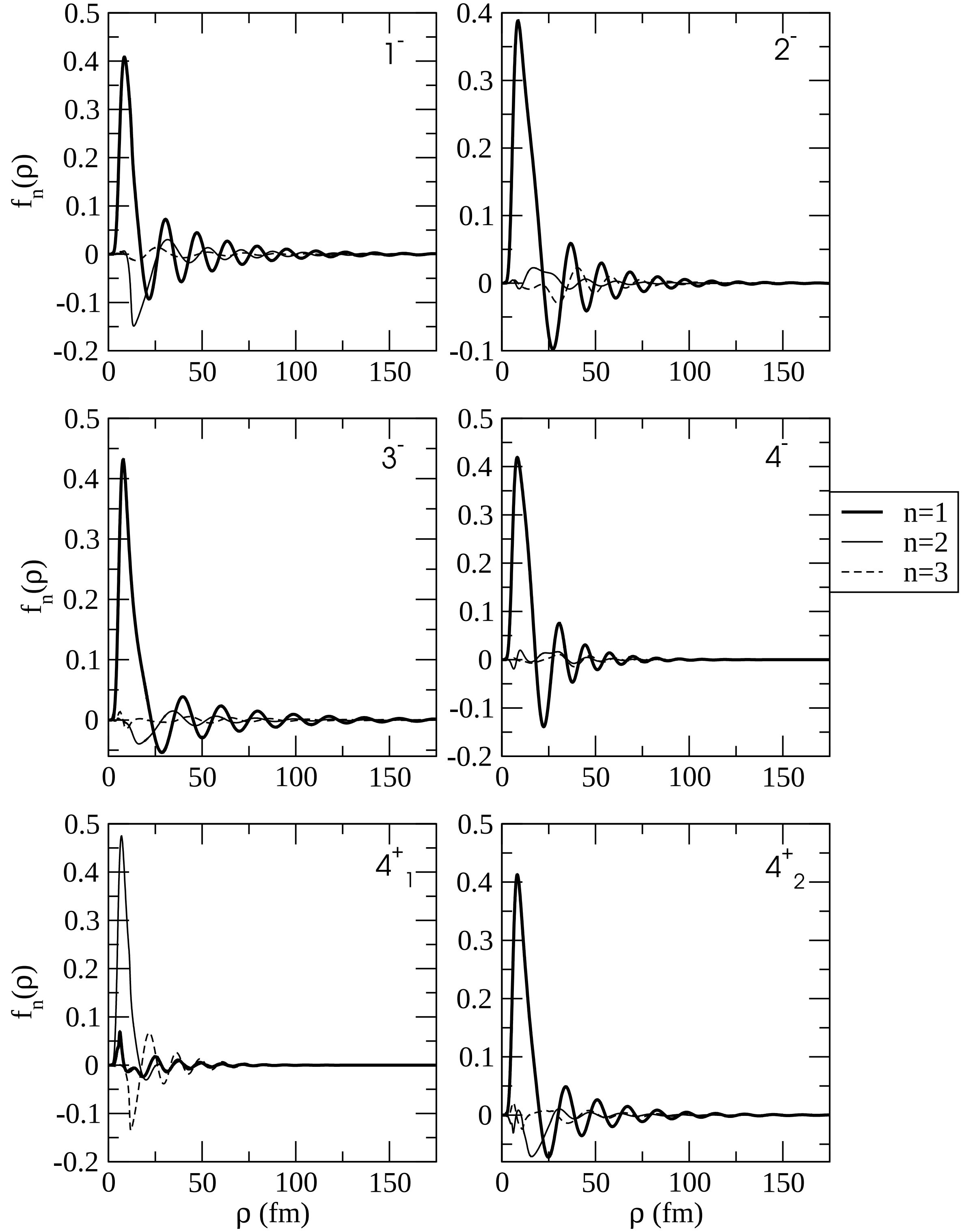

Figure 5: The real parts of the three lowest adiabatic radial wavefunctions as functions of ρ for the ^{12}C resonances with J^{π}.

$\Psi(\boldsymbol{x}, \boldsymbol{y}) = \Sigma_n \, f_n(\rho)\Phi_n(\rho, \Omega)$

Each fall off exponentially while oscillating around zero

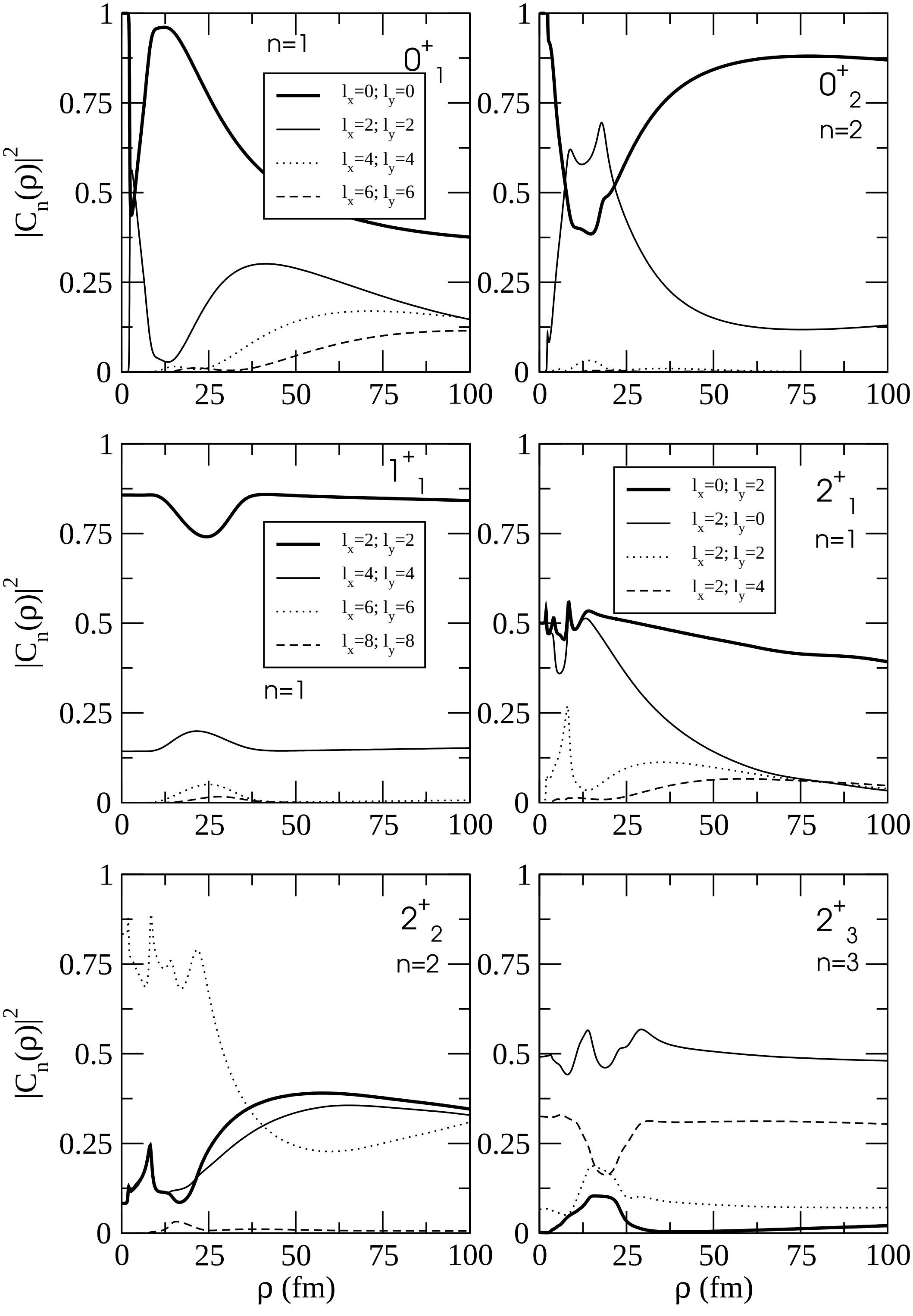

Figure 6: The partial wave decomposition of the ^{12}C resonances with J^π as indicated on the figure shown as function of ρ for the dominating adiabatic eigenvalue.

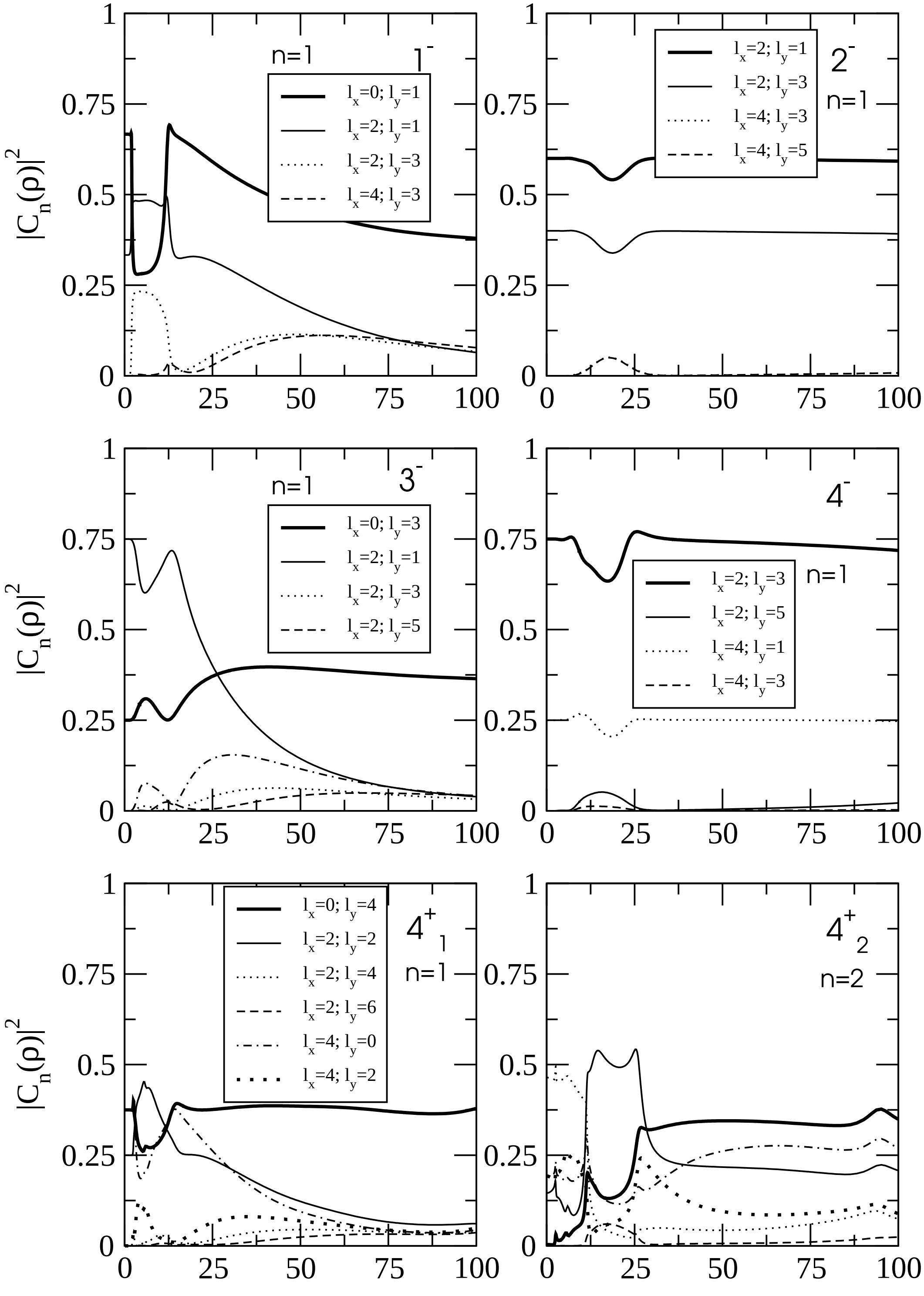

Figure 7: The partial wave decomposition of the ^{12}C resonances with J^π as indicated on the figure shown as function of ρ for the dominating adiabatic eigenvalue.

Table 1: Components included in the three-body calculations have $K_{max} = 20$ except those specified here. The left part refers to the components in the first Jacobi set ($\boldsymbol{x}$ connecting the two nucleons), and the right part to the ones in the second and third Jacobi sets ($\boldsymbol{x}$ connecting the alpha-particle and one of the nucleons).

1^{st} Jacobi set 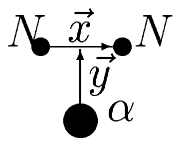						2^{nd} and 3^{rd} Jacobi sets 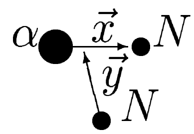					
ℓ_x	ℓ_y	L	s_x	s_y	K_{max}	ℓ_x	ℓ_y	L	s_x	s_y	K_{max}
0	2	2	0	0	180	0	2	2	1/2	0	44
2	0	2	0	0	180	0	2	2	1/2	1	44
1	1	1	1	1	180	2	0	2	1/2	0	70
1	1	2	1	1	64	2	0	2	1/2	1	44
2	2	2	0	0	90	1	1	1	1/2	1	240
1	3	2	1	1	42	1	1	2	1/2	0	240
3	1	2	1	1	42	1	1	2	1/2	1	44
2	4	2	0	0	54	2	2	1	1/2	1	32
4	2	2	0	0	54	2	2	2	1/2	0	50
4	4	2	0	0	68	2	2	2	1/2	1	42
						1	3	2	1/2	0	42
						1	3	2	1/2	1	42

Notice Jacobi coordinates

Each of the Faddeev components are partial wave expanded

Rather large K_{max} in each of these many partial waves

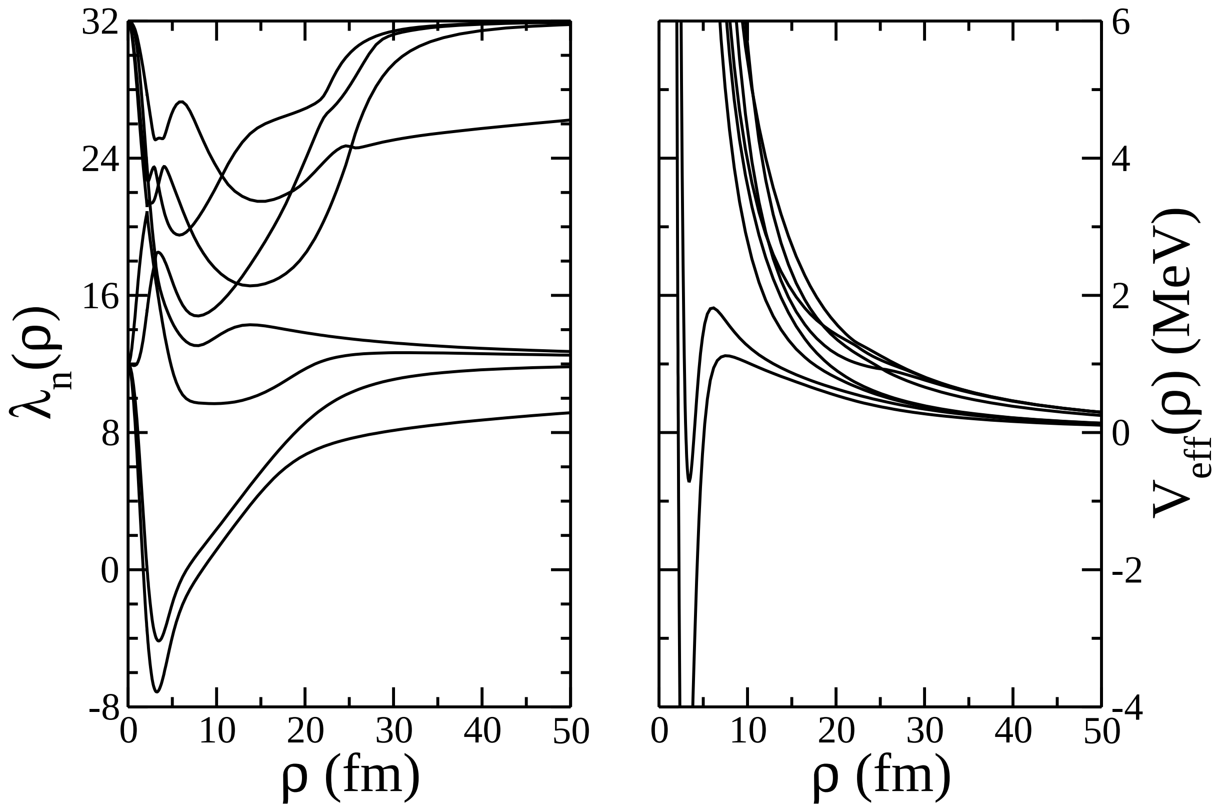

Figure 8: The real parts of the lowest 8 angular eigenvalues (left) and corresponding adiabatic potentials (right) as functions of ρ for the 2^+ states in ^{6}He (^{4}He + n + n). The scaling angle is $\theta = 0.10$.

Effective hyperradial potentials
Attractive region and a barrier

Resonance properties:
Energy determined by attractive pocket
Width determined by the barrier
Large-distance behavior determines final state energy distribution

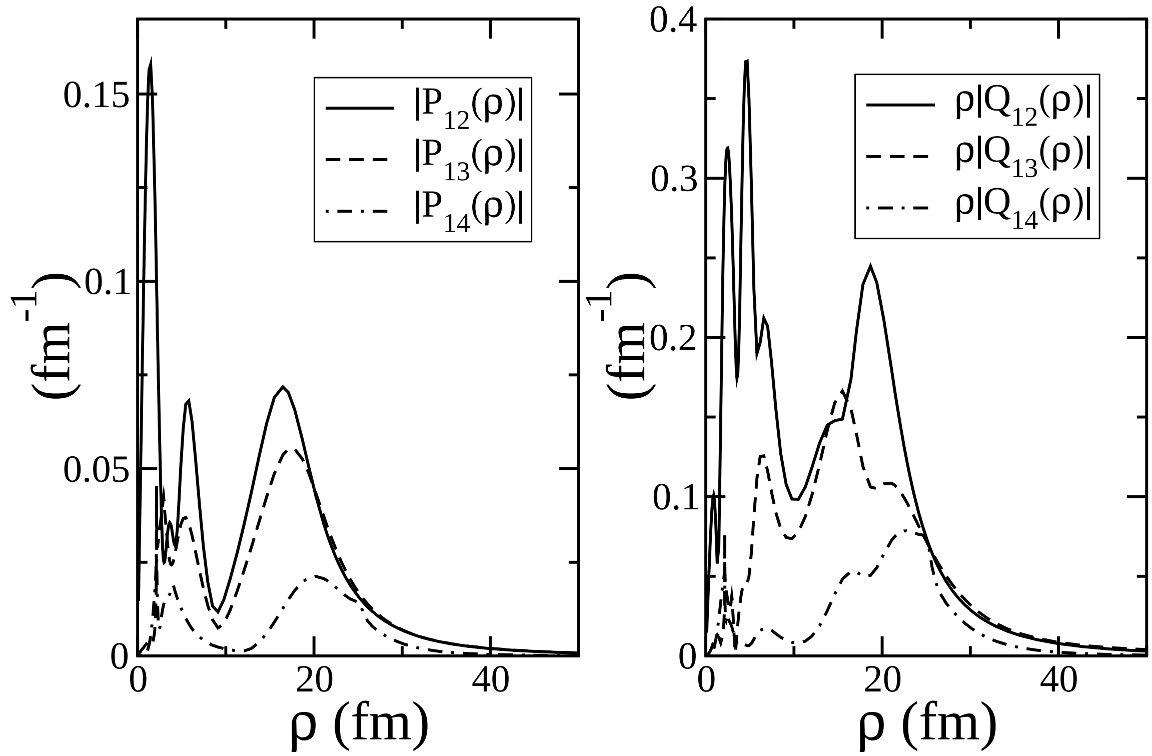

Figure 9: The coupling potentials between the four lowest adiabatic levels for $\theta = 0.10$ shown as functions of ρ for ^{6}He(2^+). The first and the fourth levels have similar quantum numbers but approach the $K = 2$ and 4 levels, respectively. To show the first (P) and second (Q) order coupling potentials in the same units (fm^{-1}) we multiply Q by ρ. (The energy unit is restored in the coupling potentials by including the omitted factor, i.e. $\hbar^2 Q/(2m)$, $\hbar^2 P/(2m)\partial/\partial\rho$).

Couplings determine relative size of radial wavefunctions
Fall off at intermediate distance
Numerical stability at large distance
Compromise between:
lowest (adiabatic) state and maintaining the structure

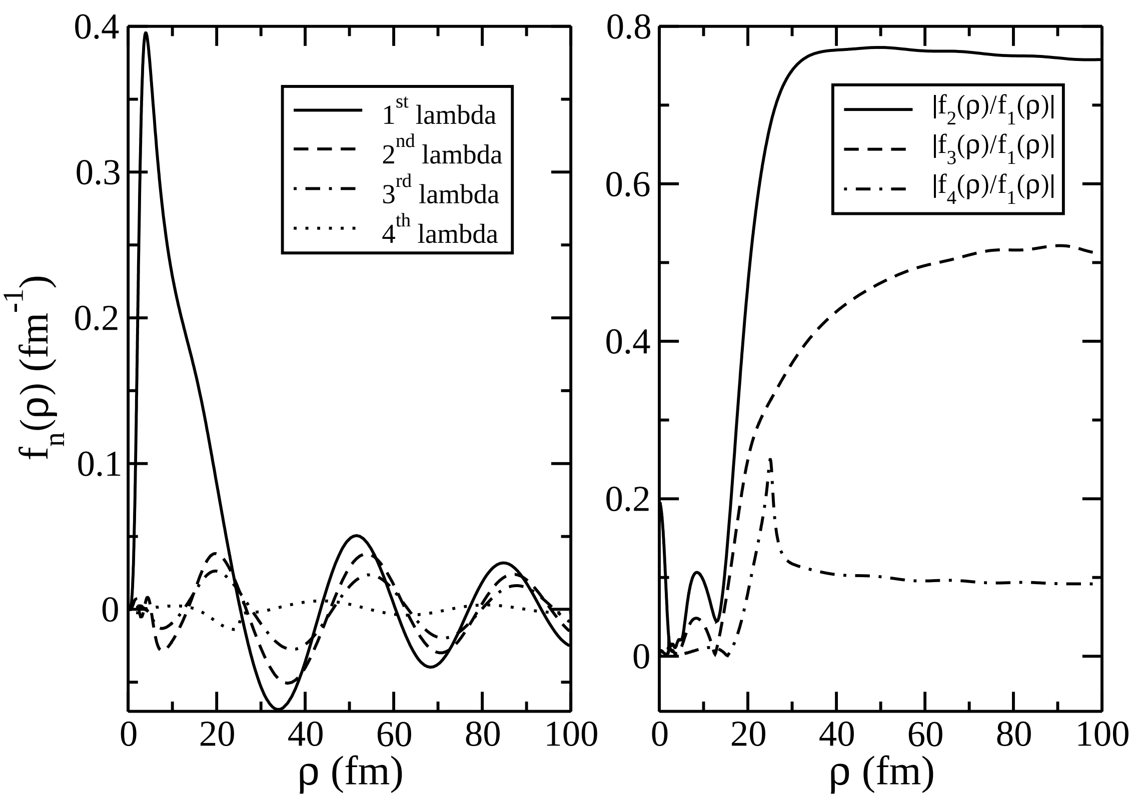

Figure 10: The lowest four radial wavefunctions (left) and their relative sizes (right) for $\theta = 0.10$ as functions ρ for the ^{6}He(2^+) resonance.

$\Psi(\boldsymbol{x}, \boldsymbol{y}) = \Sigma_n f_n(\rho)\Phi_n(\rho, \Omega)$

Each fall off exponentially while oscillating around zero
Relative size at large distance is stable
Determine energy distribution

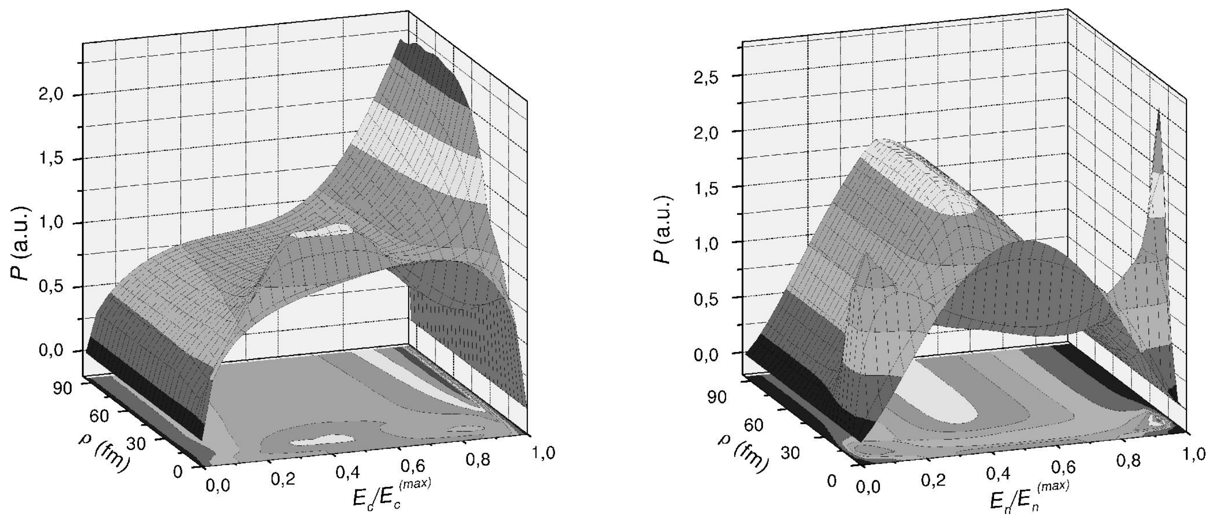

Figure 11: The energy distributions of neutrons and α-particles after decay of ^{6}He(2^+) for $\theta = 0.10$. The three-dimensional plot show the dependence on ρ with inclusion of 8 adiabatic wavefunctions. The maximum energies are $(m_\alpha + m_n)/(m_\alpha + 2m_n)E_0$ and $2m_n/(m_\alpha+2m_n)E_0$ for the neutron and the α-particle, respectively. Here E_0 is the energy of the decaying resonance.

Kinetic energy distribution of third particle:

$$P(k_y^2) \propto P(\cos^2\alpha) \propto \sin(2\alpha) \int d\Omega_x d\Omega_y |\Psi(\rho, \alpha, \Omega_x, \Omega_y)|^2$$

Neutrons peak at intermediate energy
α-particles peak at large energy
Two neutron go together, not α-neutron against neutron
Virtual neutron-neutron state is essential

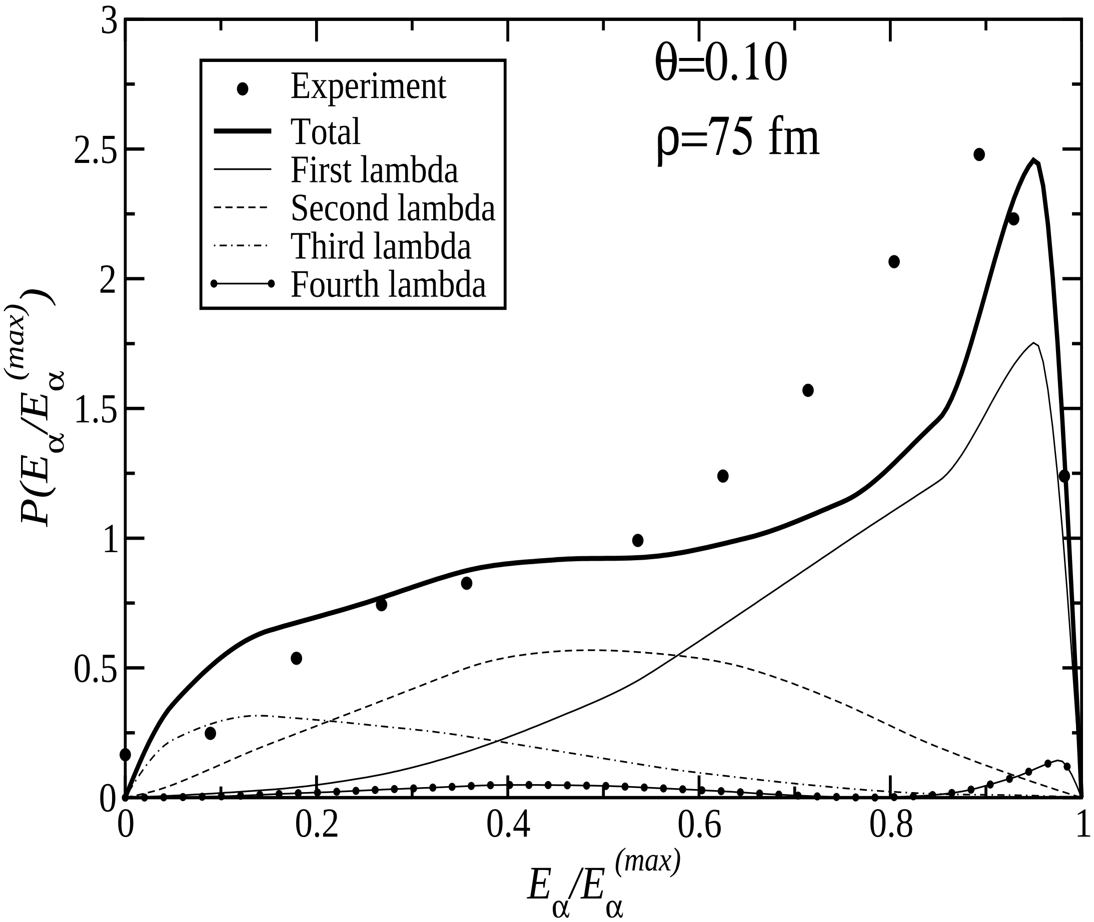

Figure 12: The energy distribution of the α-particle after decay of the 2^+-resonance in ^{6}He. The scaling angle is $\theta = 0.10$ and $\rho = 75$ fm where convergence is reached. The points are extracted from the measurements in [8]. Contributions from the lowest 4 adiabatic potentials are shown individually.

Old data
Contributions from several adiabatic potentials
Interference is important

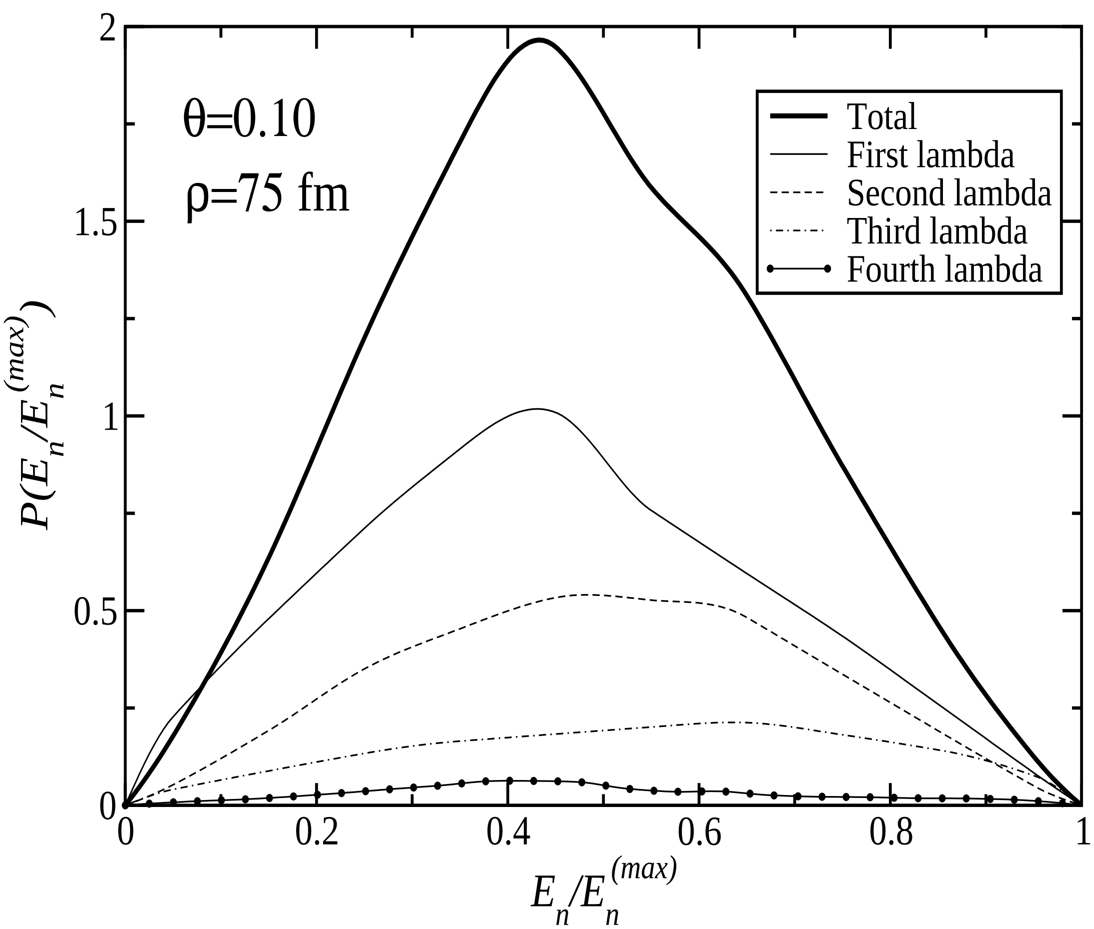

Figure 13: The energy distribution of the neutrons after decay of the 2^+-resonance in ^{6}He. The scaling angle is $\theta = 0.10$ and $\rho = 75$ fm where convergence is reached. The points are extracted from the measurements in [8]. Contributions from the lowest 4 adiabatic potentials are shown individually.

No data
Same resonance wavefunction as for α-particle

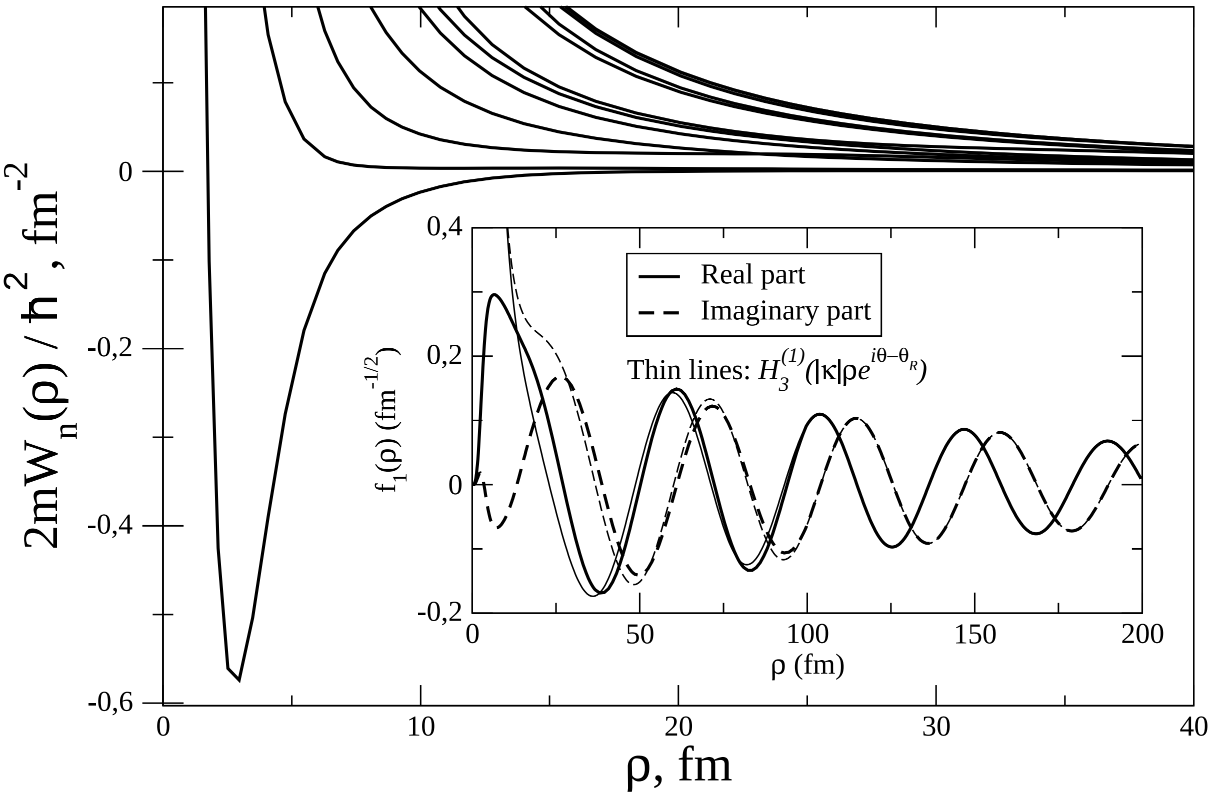

Figure 14: The lowest adiabatic potentials $W_n(\rho)$ for the ^{11}Li(1^-) halo nucleus within the three-body ^{9}Li+n+n model with interactions from [7]. The n-core and n-n scattering lengths are $a_{nc} \approx a_{nn} \approx$20 fm. The inset shows the lowest hyper-radial resonance function with its large distance asymptotics – the Hankel function. The complex scaling angle $\theta = 0.15$, the resonance angle $\theta_R = 0.12$ corresponds to the resonance energy of about $0.4 - 0.1i$ MeV.

Large scattering length
Decreasing and oscillating radial function

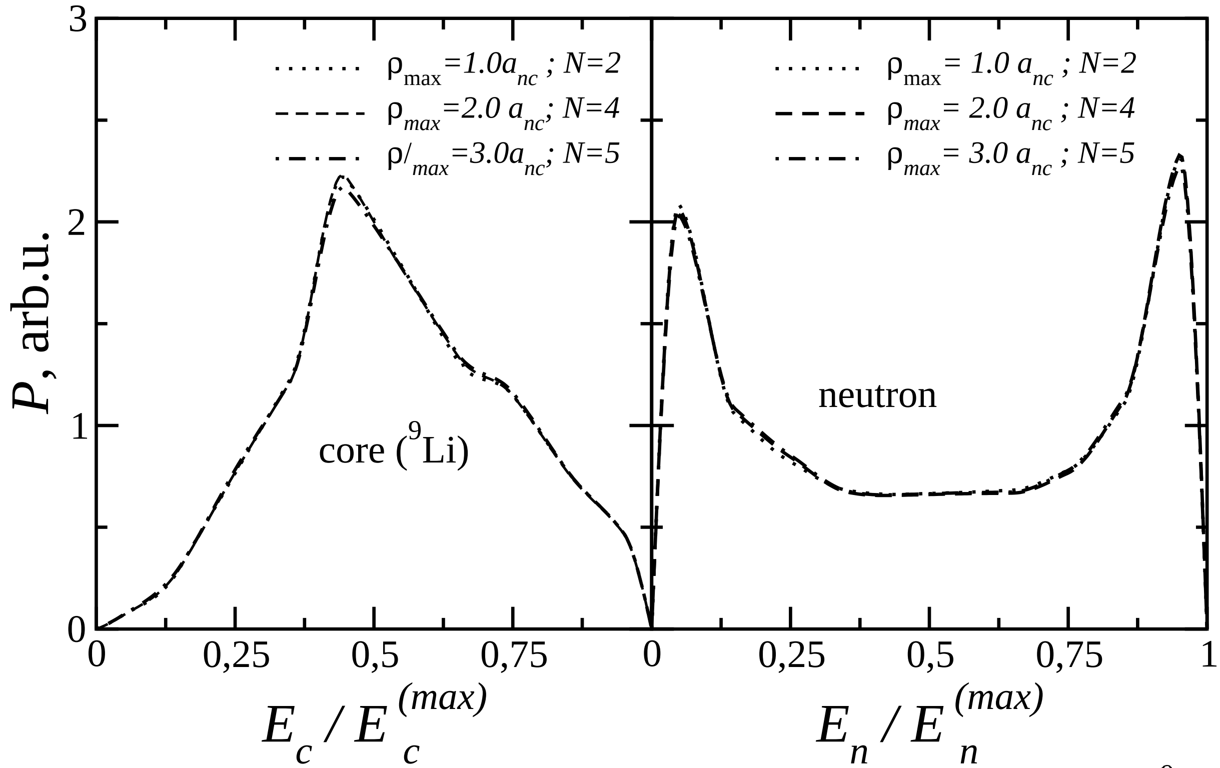

Figure 15: The energy distributions of the fragments - the core, ^{9}Li, and the neutrons - in the decay of a three-body resonance ^{11}Li(1^-) calculated in the three-body $^9\mathrm{Li} + n + n$ model with only s-wave n-core interactions (scattering length $a_{nc} \approx 50$ fm). The different curves are calculated with different ρ_{max} and different numbers of adiabatic channels N to illustrate the convergence.

Schematic model
Only s-waves and large neutron-core scattering length
Lowest adiabatic function is very accurate
Very stable against large variation of ρ_{max}
Core distribution peaks at intermediate energies
Neutron distribution has a low and a high energy peak
Mechanism is neutron emission, high energy
Then neutron-core stick together, low energy neutron

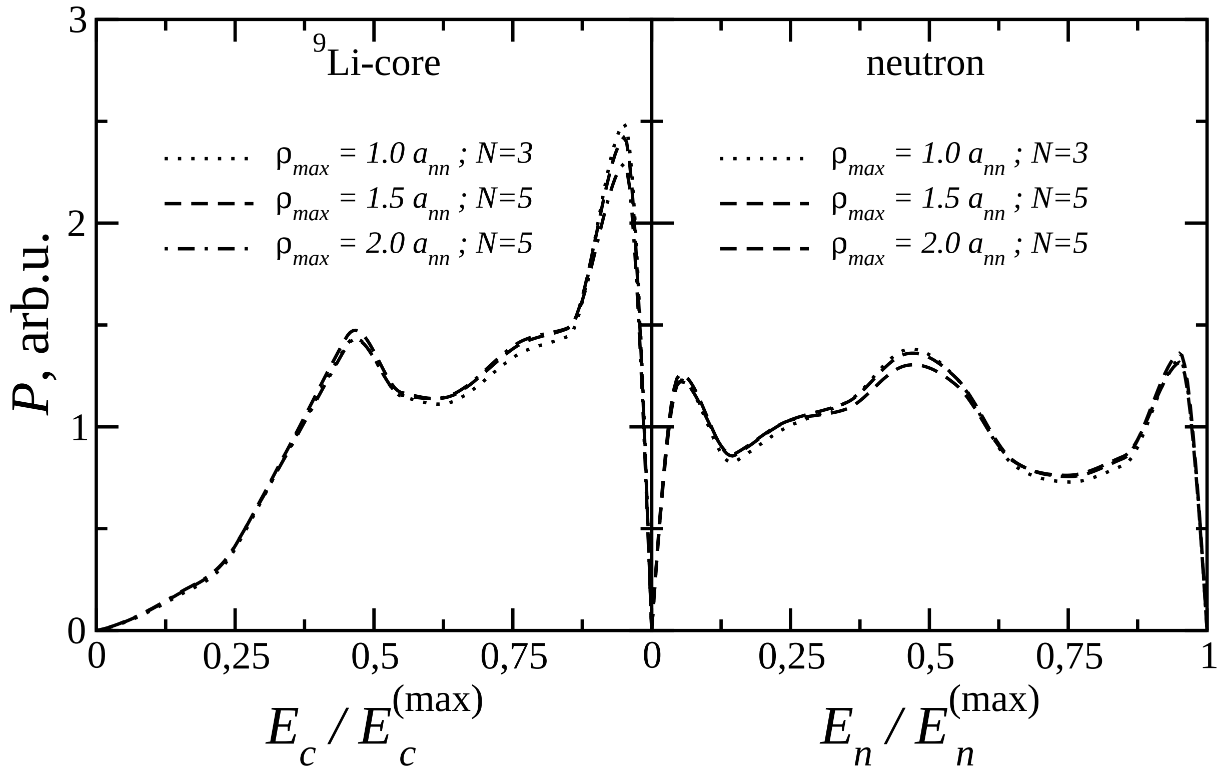

Figure 16: The energy distributions of the fragments - the core, ^{9}Li, and the neutrons - in the decay of a three-body resonance ^{11}Li(1^-) calculated in the three-body $^9\text{Li} + n + n$ model with s-wave n-core interactions (scattering length $a_{nc} \approx 50$ fm), and an s-wave interaction in the $n - n$ subsystem (scattering length $a_{nn} \approx a_{nc} \approx 50$ fm). The different curves are calculated with different ρ_{max} and different numbers of adiabatic channels N to illustrate the convergence.

Schematic model
Only s-waves, and large neutron-neutron and neutron-core scattering length
Lowest adiabatic function is very accurate
Very stable against large variation of ρ_{max}
Core distribution gets new peak at high energy
Neutron distribution gets a new peak at intermediate energy
Two coherent decay mechanisms: Neutron emission, high and low energy neutrons, intermediate core energy
Core emission, two neutrons stick together
Core energy is maximum, neutron energy is intermediate

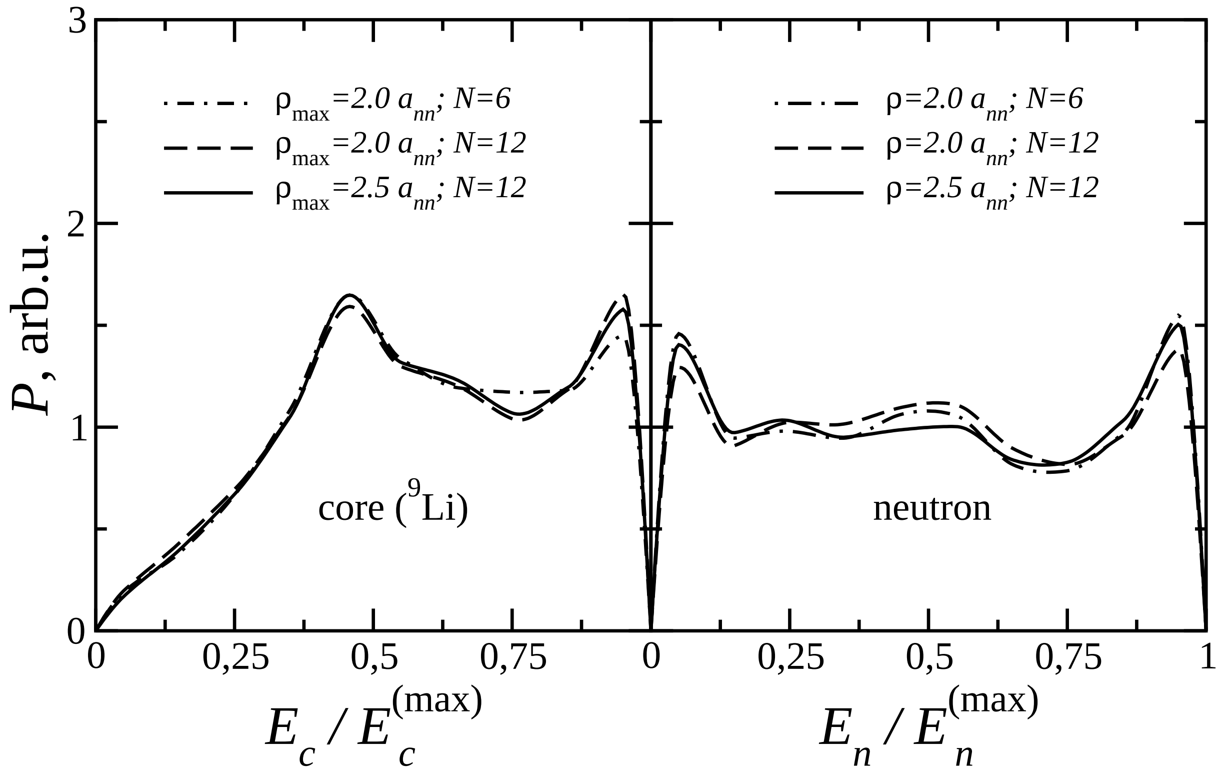

Figure 17: The energy distributions of the fragments - the core, ^9Li, and the neutrons - in the decay of a three-body resonance ^{11}Li(1^-) calculated with interactions from [7] where the n-core and n-n scattering lengths are about 20 fm.

Realistic interactions reproducing all other known ^{11}Li properties
All three scattering lengths now about 20 fm
All peaks from schematic model remains
Trace of Efimov effect

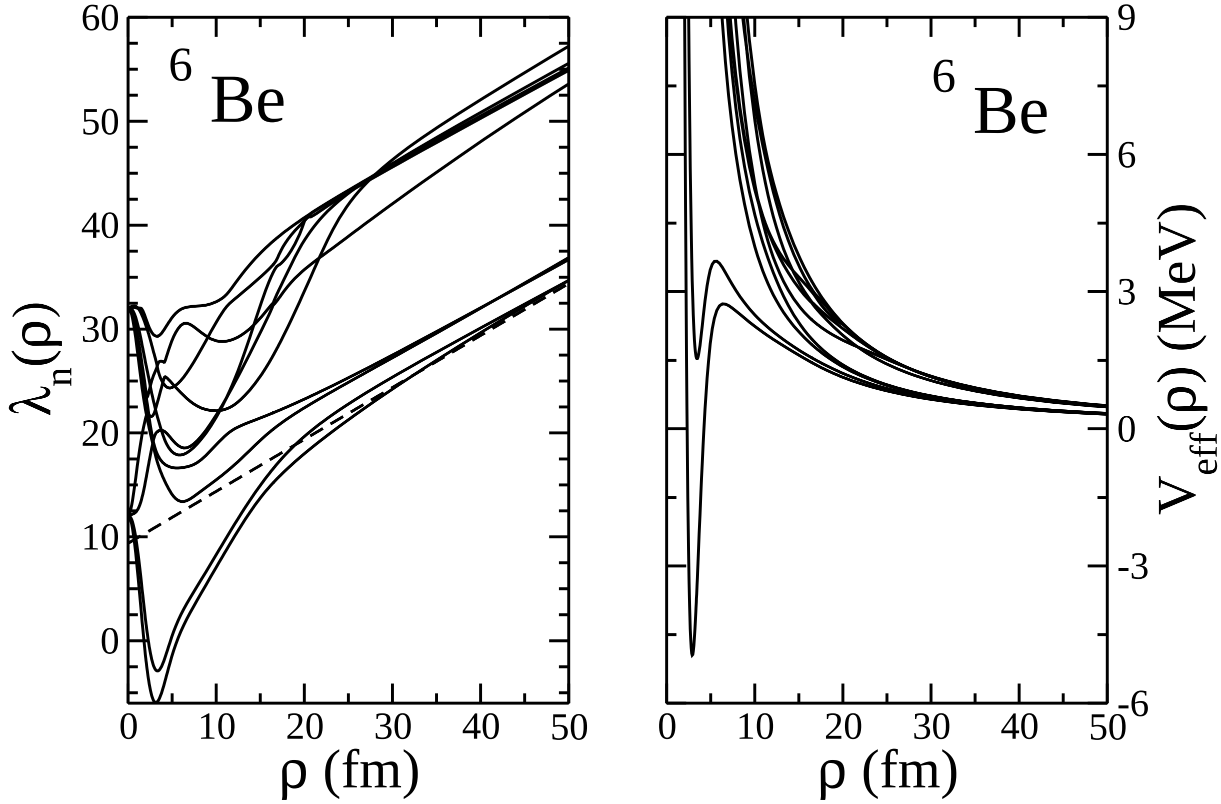

Figure 18: Real parts of the lowest 10 angular eigenvalues (left) and their corresponding adiabatic potentials (right) as functions of ρ for the 2^+-resonance in ^{6}Be. The scaling angle is $\theta = 0.15$. The dashed line is the estimated behaviour at large distances for the lowest angular eigenvalue.

The ^{6}He analog 2^+-resonance in ^{6}Be
Only difference is Coulomb
Small ρ: Same structure as for ^{6}He
For large ρ:
Angular eigenvalues: linear in ρ, Potentials: $1/\rho$

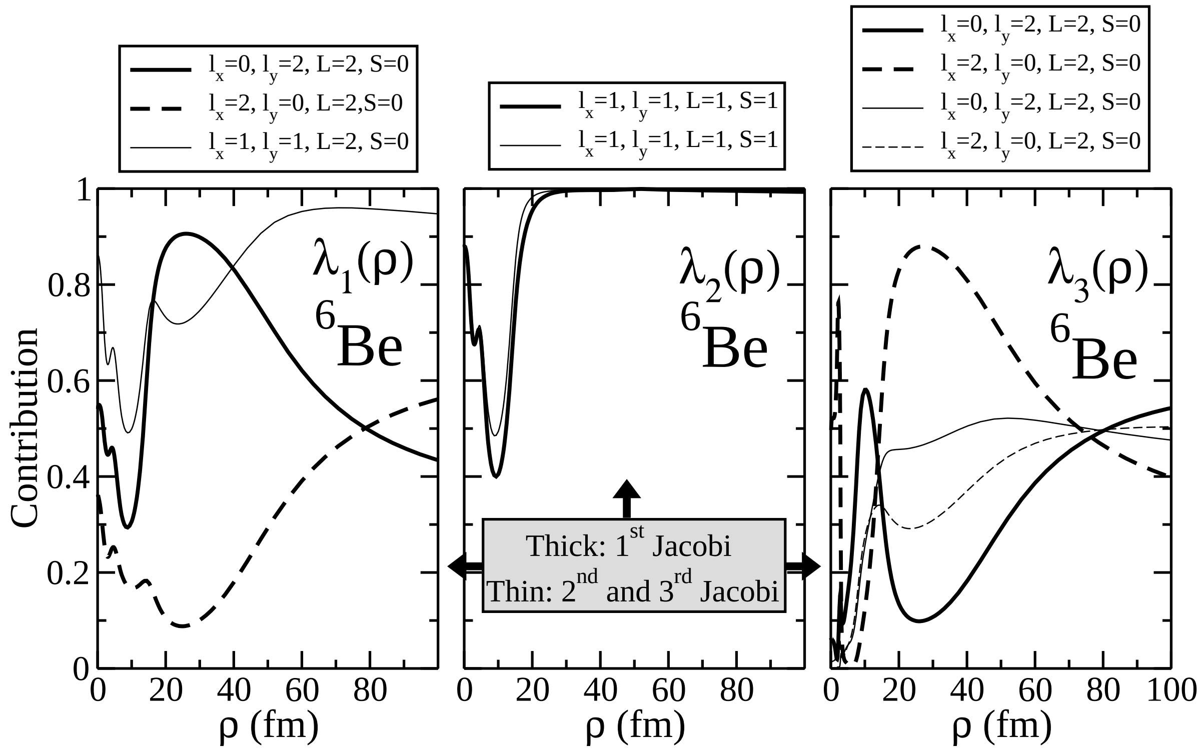

Figure 19: The fraction of the dominating components in the angular eigenfunction for the three lowest adiabatic potentials as function of ρ for ^{6}Be (2^+), see Fig. 1. The quantum numbers are as given in table 1. Thick lines: x refers to the two-proton system and y to its center of mass motion relative to the α-particle. Thin lines: x refers to the proton-α system and y to its center of mass motion relative to the other proton.

Partial wave decomposition of angular wavefunction
Strong variation from small to large distance
First eigenvalue:
Proton-proton s-wave dominates at small distance
Proton-proton s and d-waves are comparable at large ρ
α-proton p-waves dominate at large distance

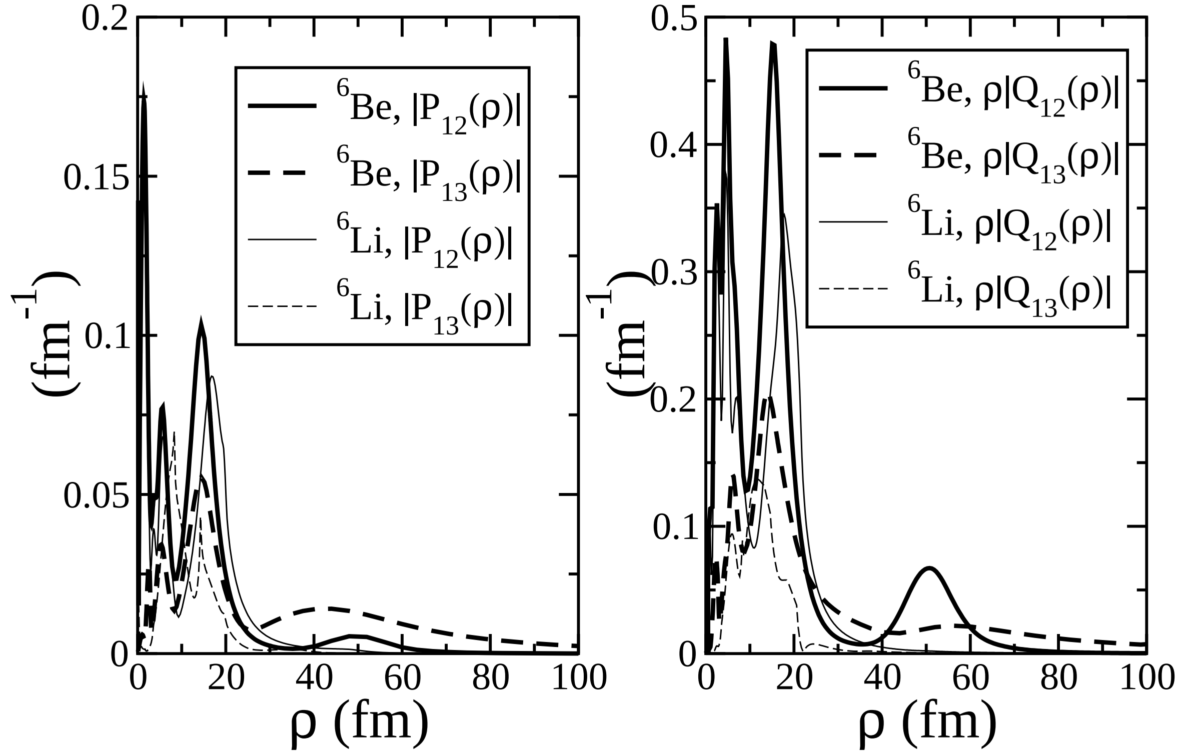

Figure 20: The absolute values of the coupling potentials between the three lowest adiabatic levels for the 2^+-resonance in ^{6}Be (thick curves $\theta = 0.15$ rads) as functions of ρ, and the corresponding isobaric analog states in ^{6}Li (thin curves $\theta = 0.10$ rads).

Couplings determine relative size of radial wavefunctions
Fall off at intermediate distance
Numerical stability at large distance

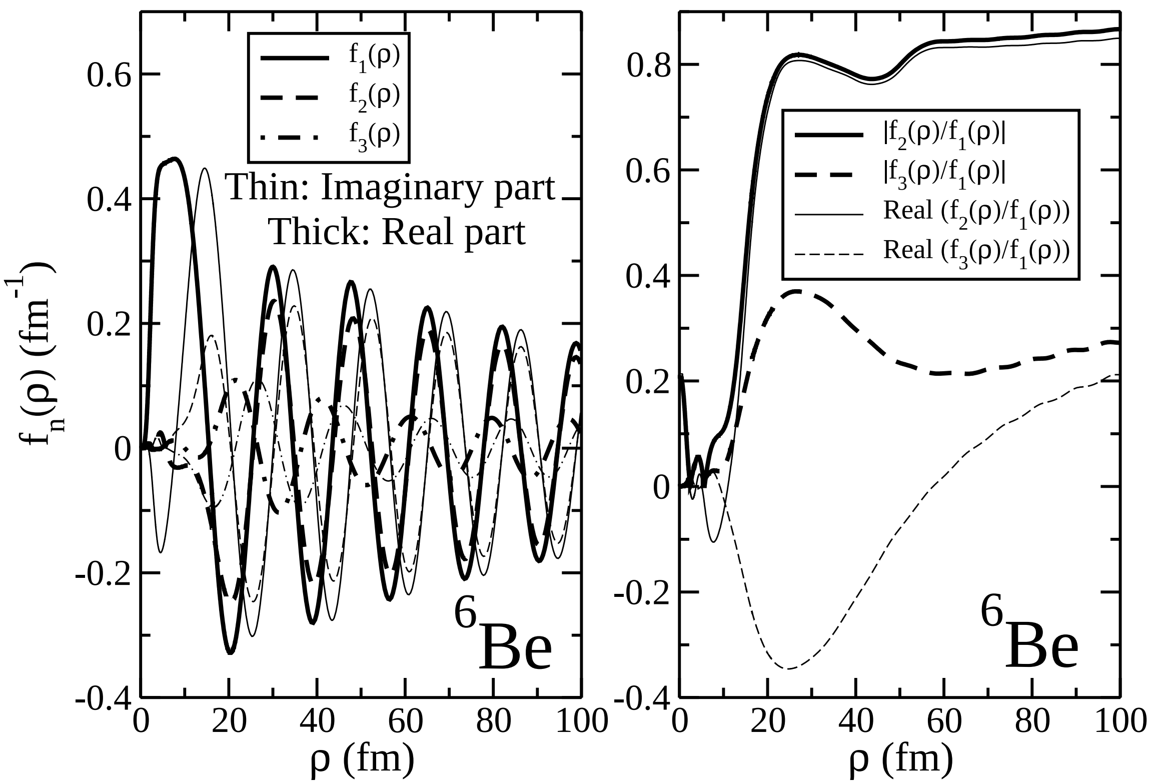

Figure 21: Left: Radial wave functions corresponding to the three first adiabatic potentials for the 2^+-resonance in ^{6}Be. The real and imaginary parts are shown by the thick and thin curves, respectively. Right: Absolute values (thick curves) and the real parts (thin curves) of the ratios between the radial wave functions. The probability distribution has for each ρ been normalized to 1 as function of α.

$\Psi(\boldsymbol{x}, \boldsymbol{y}) = \Sigma_n \, f_n(\rho) \Phi_n(\rho, \Omega)$

Each fall off exponentially while oscillating around zero
Relative size at large distance determine energy distribution
Numerical stability is not obvious

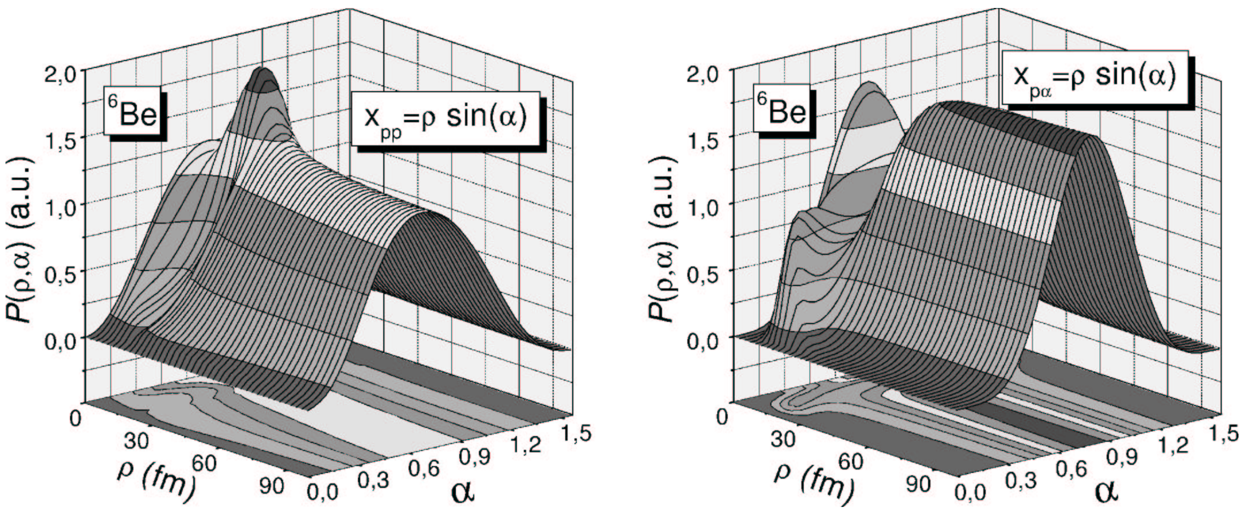

Figure 22: The probability distribution for the 2^+-resonance in ^{6}Be including the lowest 10 adiabatic potentials as function of the hyperradius ρ and hyperangle α related to the distance by $r_{ik} \propto \rho \sin\alpha$, i.e. the distance between either the one proton and core r_{pc} (right) or the two protons r_{pp} (left).

Structure of total resonance wavefunction
Vary strongly from small to large distance
Stable at larger distance
Much better than indicated by the first radial wavefunctions

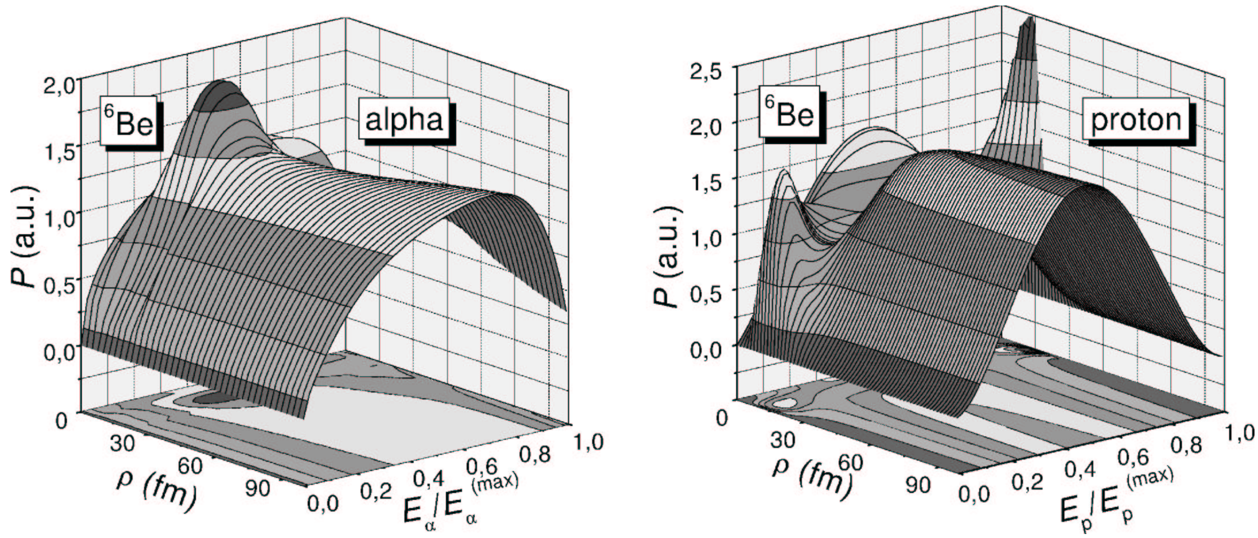

Figure 23: Kinetic energy distributions of protons (right) and α-particles (left) after decay of the 2^+-resonance in ^{6}Be. The three-dimensional plots show the dependence on ρ with inclusion of 10 adiabatic wave functions as function of $\cos^2\alpha$, i.e. the kinetic energies $E_{\alpha,p}$ are in units of their maximum values $E_{\alpha,p}^{(max)}$ given by $(m_\alpha + m_p)/(m_\alpha + 2m_p)E_R$ and $2m_p/(m_\alpha + 2m_p)E_R$ for the proton and the α-particle, respectively, where E_R is the energy of the decaying resonance.

Kinetic energy distribution of third particle:
$P(k_y^2) \propto P(\cos^2\alpha) \propto \sin(2\alpha) \int d\Omega_x d\Omega_y |\Psi(\rho, \alpha, \Omega_x, \Omega_y)|^2$
Protons peak at intermediate energy
α-particles with broad peak tilted towards large energy
Coulomb is coupling a lot and broadening distributions
Virtual proton-proton state is not present or very weak

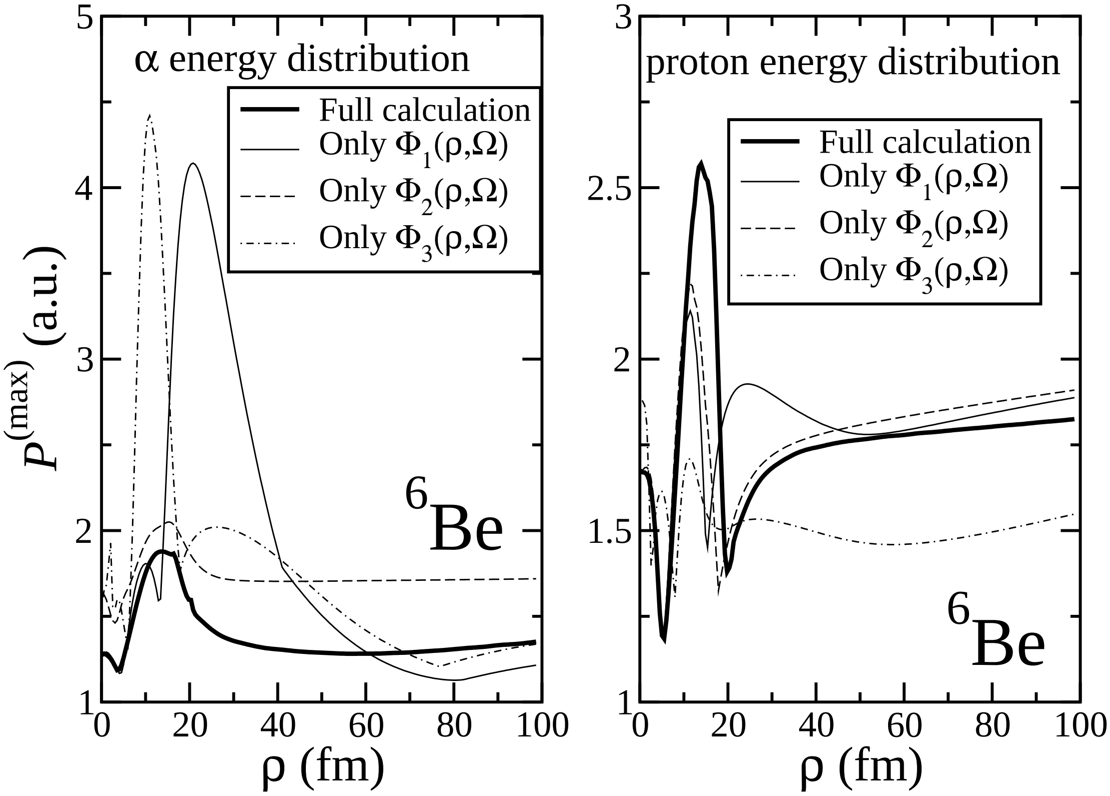

Figure 24: Projections of kinetic energy distributions for ^{6}Be-decay. Thick curves: Projection of the α (left panel) and proton (right panel) kinetic energy distributions Fig.(23) on the $E_{\alpha,p}/E_{\alpha,p}^{(max)} = 1$ plane. They are then the profile originating from the maximum values of the energy distribution for each value of ρ. The thin curves are the same profile but when respectively only the first adiabatic term (solid), only the second adiabatic term (dashed), or only the third adiabatic term (dot-dashed) is included in the calculation.

The kinetic energy distribution is redistributed with ρ
The total distribution is much more stable (thick curves)

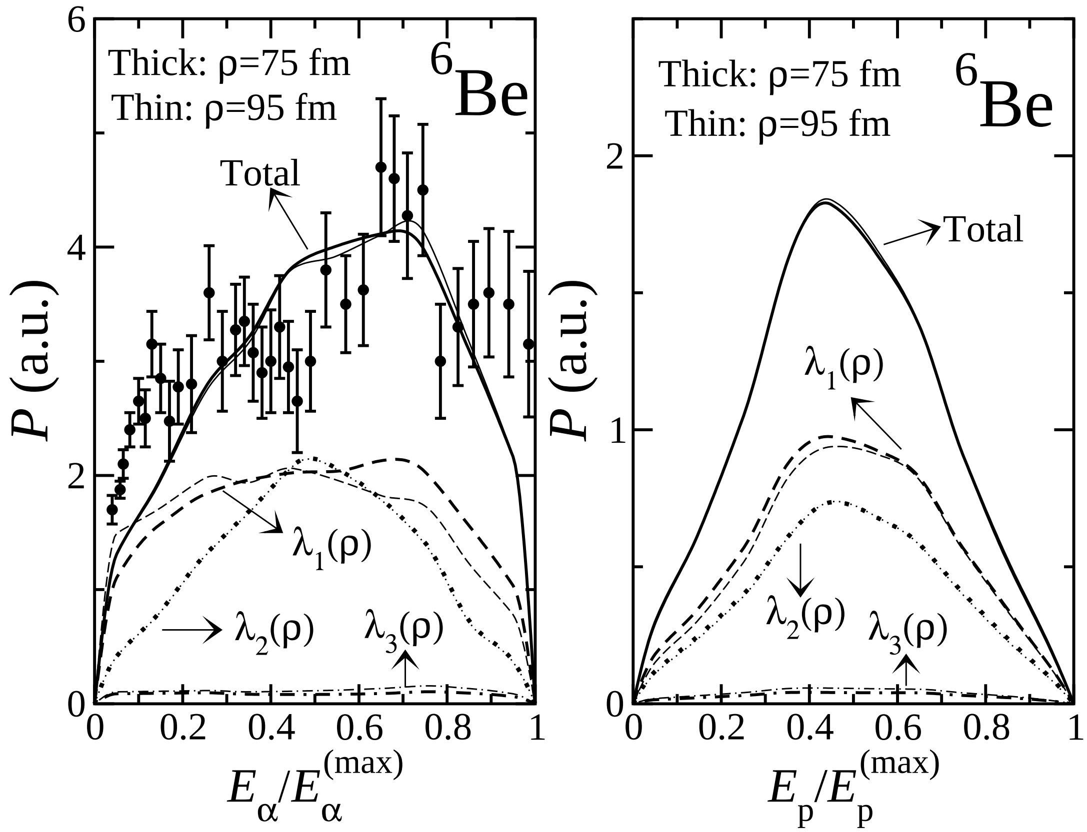

Figure 25: The kinetic energy distribution of the α-particle (upper part) and the proton (lower part) after decay of the 2^+-resonance in ^{6}Be. The scaling angle is $\theta = 0.15$ and the two sets of curves are for $\rho = 75, 95$ fm. The points are extracted from the measurements in [8]. Contributions from the lowest adiabatic potentials are shown individually.

Old data for α-particle
Contributions from several adiabatic potentials

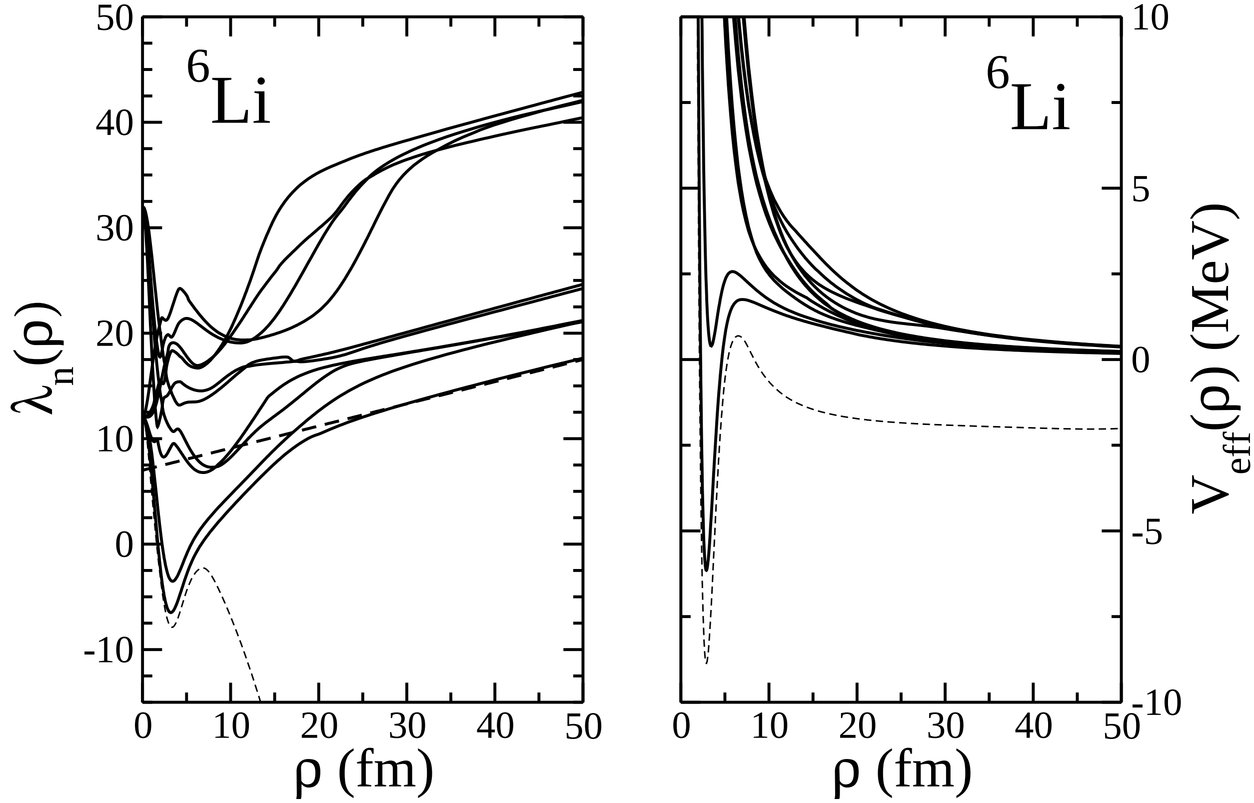

Figure 26: Real parts of the lowest 10 angular eigenvalues (left) and their corresponding adiabatic potentials (right) as functions of ρ for the 2^+-resonance in ^{6}Li. The scaling angle is $\theta = 0.10$. The dashed line is the estimated behaviour at large distances for the lowest angular eigenvalue.

The ^{6}He analog 2^+-resonance in ^{6}Li
Only difference is Coulomb
Small ρ: Same structure as for ^{6}He
For large ρ:
Angular eigenvalues: linear in ρ, Potentials: $1/\rho$
One more state:
α-deuteron structure, eigenvalue as $-\rho^2$, potential to constant

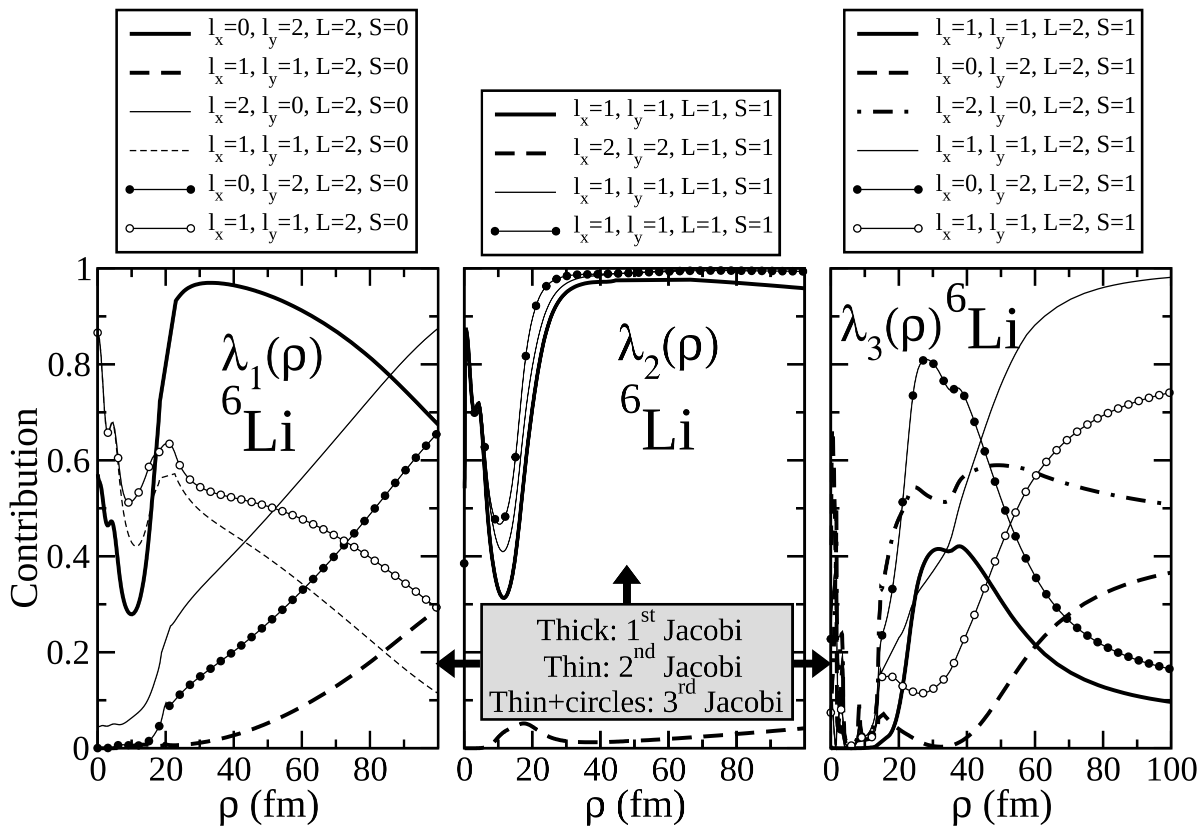

Figure 27: The fraction of the dominating components in the angular eigenfunction for the three lowest adiabatic potentials as function of ρ for ^{6}Li (2^+). The quantum numbers are as given in table 1. We omitted the almost decoupled lowest eigenfunction of deuteron-α character. In the second Jacobi set (thin lines) the x refers to the proton-α system and y to its center of mass motion relative to the neutron. In the third Jacobi set (thin+circle lines) the x refers to the neutron-α system and y to its center of mass motion relative to the proton.

Partial wave decomposition of angular wavefunction
Strong variation from small to large distance
First eigenvalue:
Proton-proton s-wave vary but dominates at all distances
Proton-proton p-wave increases with ρ, isospin 0 increase with ρ
α-proton d-wave dominates at large distance

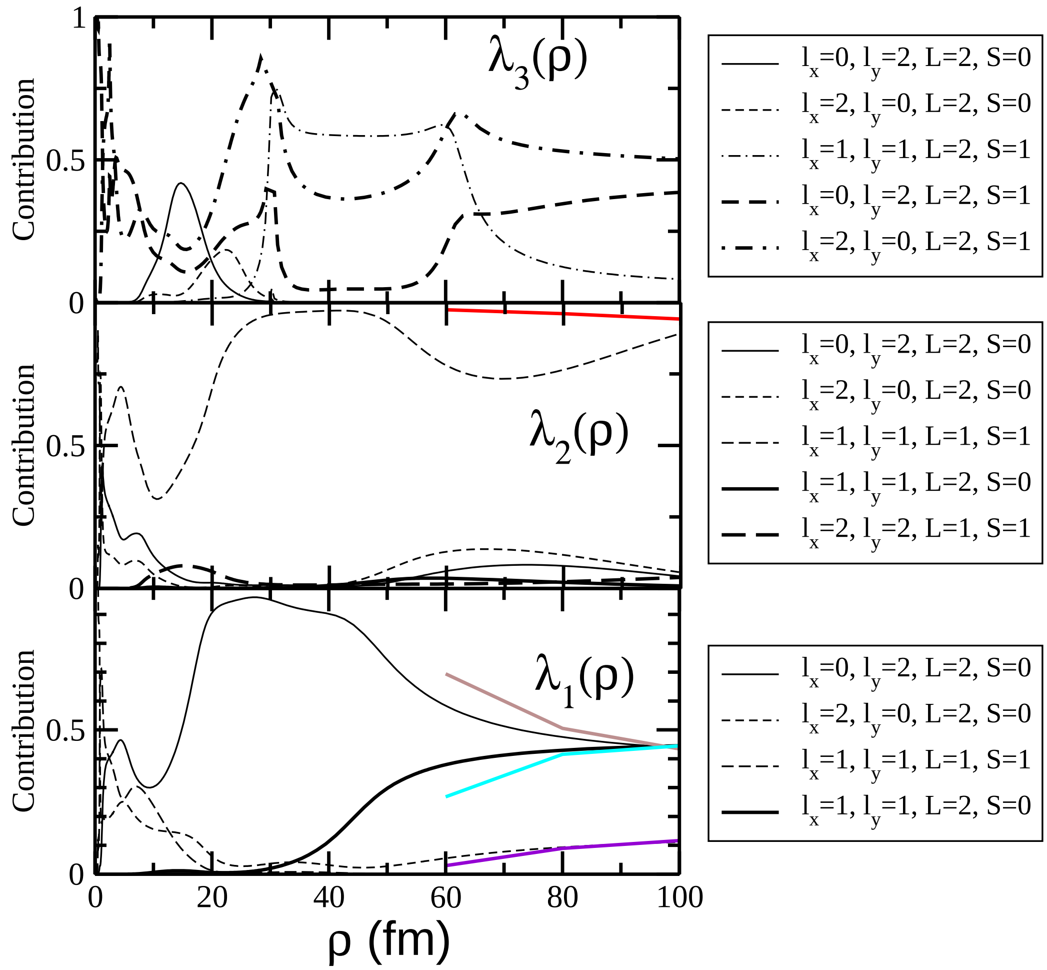

Figure 28: The fraction of the dominating components in the angular eigenfunction for the three lowest adiabatic potentials as function of ρ for ^{6}Li (2^+). The same as the previous figure for the Argonne potential.
First eigenvalue:
Proton-proton p-wave increases with ρ, isospin 0 increase with ρ
Much larger basis at large distance changes numerical values but maintain the picture. Second lambda remains as for $\rho \approx 50$ fm.

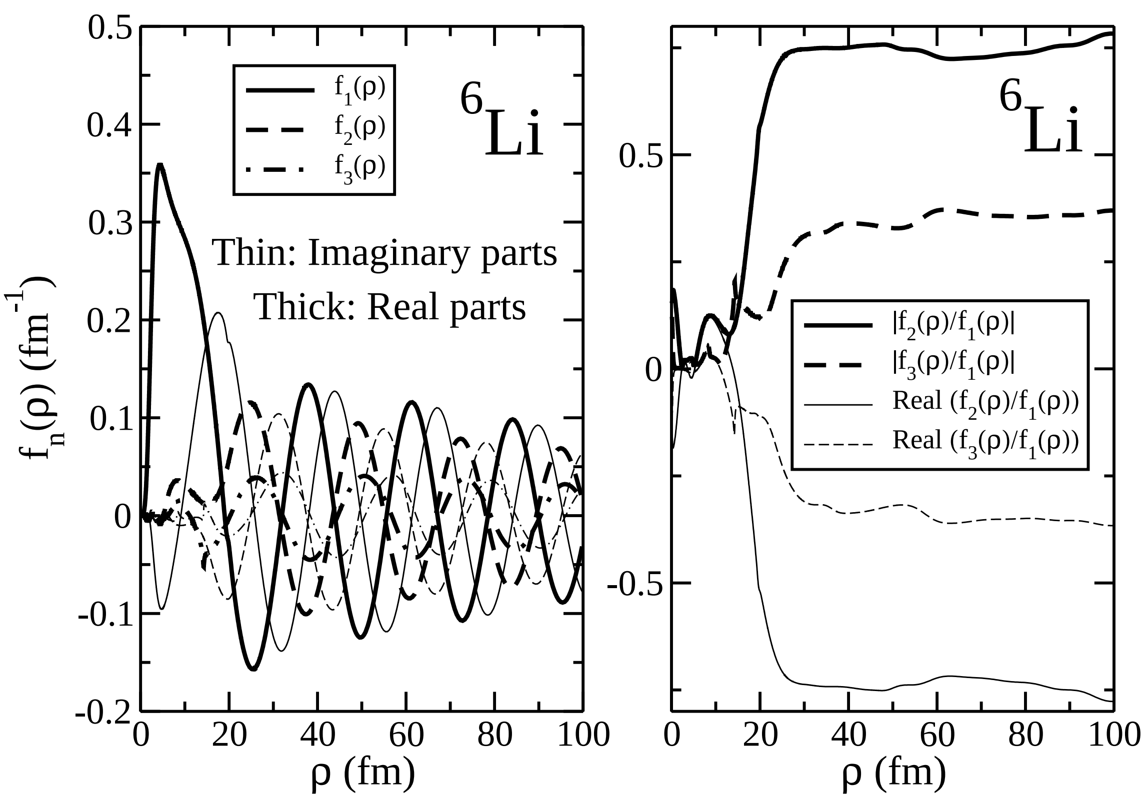

Figure 29: Left: Radial wave functions corresponding to the three first adiabatic potentials for the 2^+-resonance in ^{6}Li. The real and imaginary parts are shown by the thick and thin curves, respectively. Right: Absolute values (thick curves) and the real parts (thin curves) of the ratios between the radial wave functions. The probability distribution has for each ρ been normalized to 1 as function of α.

Each fall off exponentially while oscillating around zero
Relative size at large distance determine energy distribution
Numerical stability is established

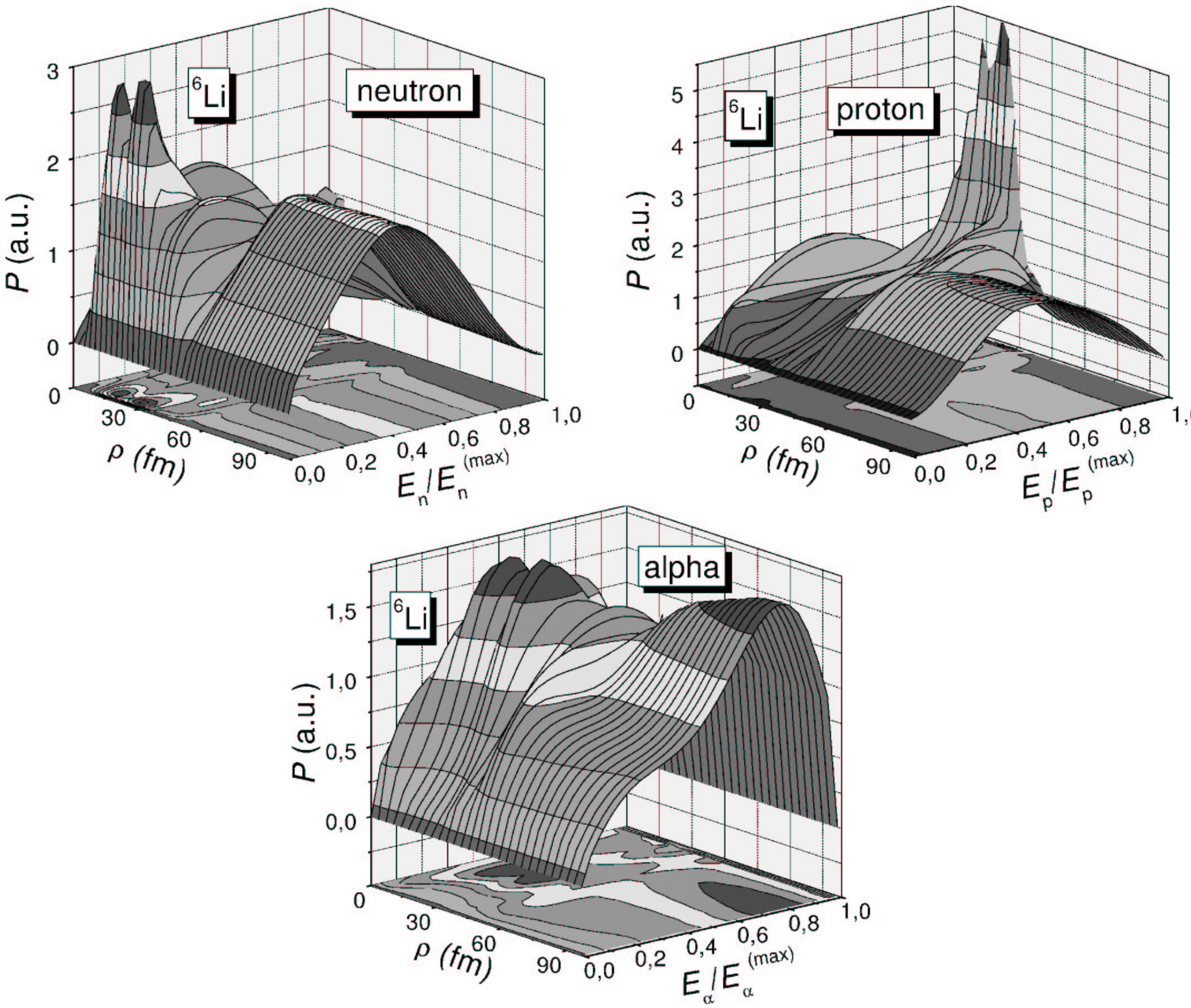

Figure 30: Kinetic energy distributions of protons (upper-right panel), neutrons (upper-left panel), and α-particles (lower panel) after decay of the 2^+-resonance in ^{6}Li corresponding to that of Fig. 10. The three-dimensional plot show the dependence on ρ with inclusion of 10 adiabatic wave functions. The maximum energies $E_{n,p,\alpha}^{(max)}$ are $(m_\alpha + m_p)/(m_\alpha + m_n + m_p)E_R$, $(m_\alpha + m_n)/(m_\alpha + m_n + m_p)E_R$ and $(m_n+m_p)/(m_\alpha+m_n+m_p)E_R$ for the neutron, the proton, and the α-particle, respectively, where E_R is the energy of the decaying resonance.

Kinetic energy distribution of third particle:
$P(k_y^2) \propto P(\cos^2\alpha) \propto \sin(2\alpha) \int d\Omega_x d\Omega_y |\Psi(\rho,\alpha,\Omega_x,\Omega_y)|^2$
Protons peak at intermediate (higher) energy
Neutrons peak at intermediate (lower) energy
α-particles with broad peak towards large energy
Neutron and proton tend to go together
Virtual neutron-proton state is active
Coulomb is broadening distributions

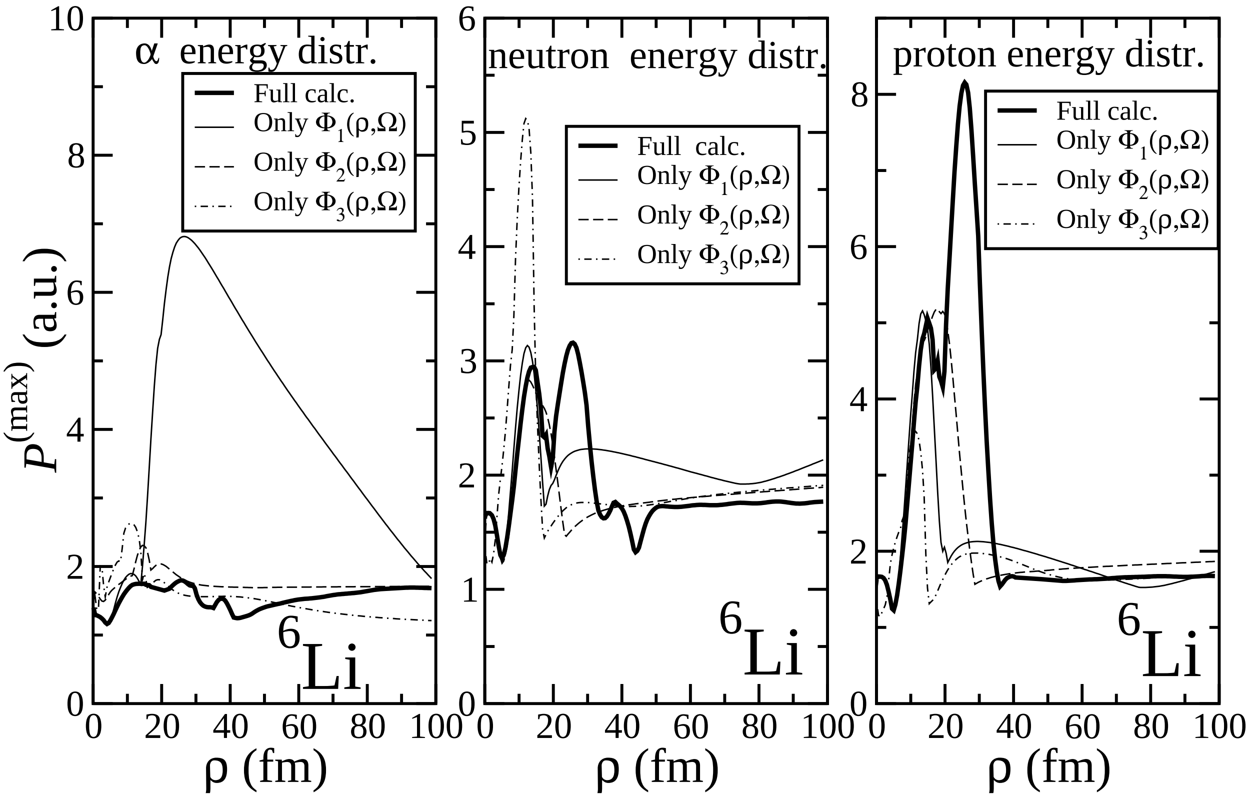

Figure 31: Projections of kinetic energy distributions as functions of ρ for ^{6}Li(2^+). Thick curves: Projection of the α (left panel) and proton (right panel) kinetic energy distributions (Fig. 10) on the $E_{\alpha,p}/E^{(max)}_{\alpha,p} = 1$ plane. They are then the profile originated by the maximum values of the energy distribution for each value of ρ. The thin curves are the same profile but when only the first adiabatic term (solid), only the second adiabatic term (dashed), or only the third adiabatic term (dot-dashed) is included in the calculation.

The kinetic energy distribution is redistributed with ρ
The total distribution is much more stable (thick curves)

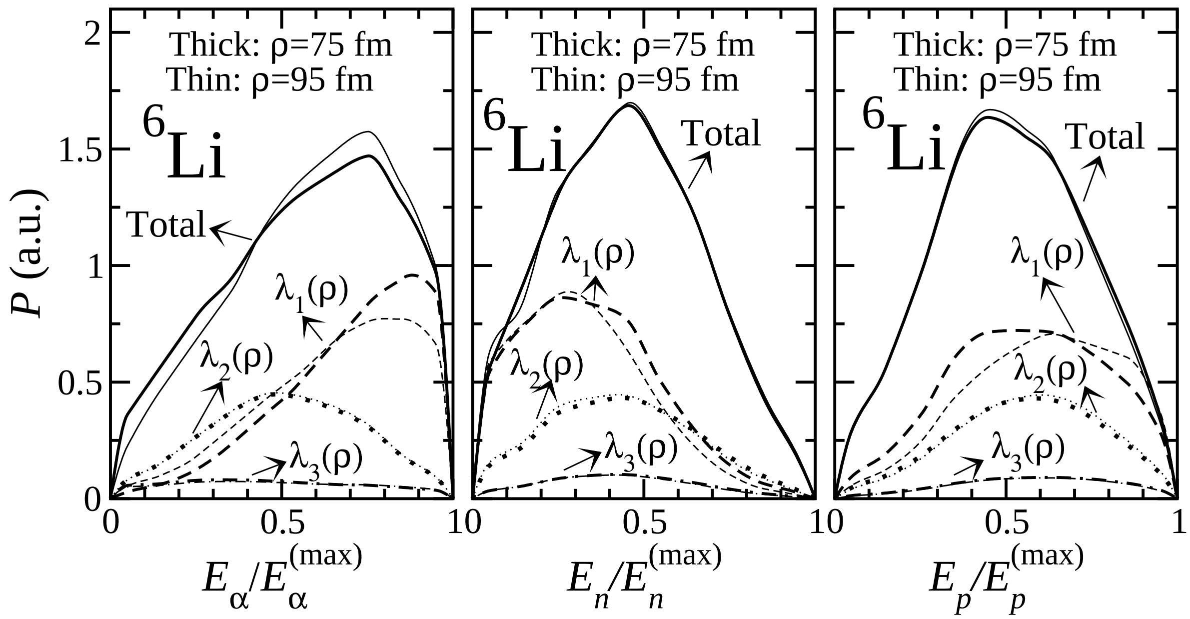

Figure 32: The kinetic energy distribution of the α-particle (upper part), the neutron (middle part) and the proton (lower part) after decay of the isobaric analog 2^+-resonance in ^{6}Li. The scaling angle is $\theta = 0.10$ and the two sets of curves are for $\rho = 75, 95$ fm. The points are extracted from the measurements in [8]. Contributions from the lowest adiabatic potentials are shown individually.

Old data for α-particle exist in another frame
Contributions from several adiabatic components
Protons peak at intermediate (higher) energy
Neutrons peak at intermediate (lower) energy
α-particles with broad peak towards large energy
Neutron and proton tend to go together
Virtual neutron-proton state is active
Coulomb is broadening the distributions

CONCLUSIONS

1. Three-body decay of many-body resonances

2. A model working in practice

3. Energies must be artificially adjusted as in α-decay

4. Width is estimated as hyperspherical barrier penetrability

5. Asymptotic wavefunction behavior determines the final state energy distributions

6. Asymptotics are established at intermediate distances where basis size is manageable

7. Large scattering lengths can be handled, Efimov effect

8. Coulomb can be handled in the cases investigated

9. Isospin mixing is a dynamic effect occurring outside the range of short-range interactions

DIFFERENCES TO GRIGORENKO ET AL

1. The spin dependence of the proton-core interaction in ^{17}Ne computations is in conflict with the mean-field spin-orbit interaction, i.e. the valence $d_{3/2}$ and $d_{5/2}$ states can not be independently populated, only specific combinations. Same problem in ^{19}Mg and ^{45}Fe. Maybe corrected later on.

2. The hyperspherical method with only one Faddeev component is used, i.e. it is not possible to describe (i) Efimov effect, (ii) close to Efimov structure, (iii) two simultaneous 2-body substructures, (iv) one 2-body resonance unless, as he sometimes does, allow this structure as a variational degree of freedom.

3. The hyperspherical method has rather small $Kmax \simeq 20-25$. With three Faddeev components we need at least $Kmax \simeq 100-150$ with only the short range interaction. The Coulomb interaction and the unavoidable couplings at large distances does not reduce the required basis size.

4. The three-body interaction is ρ^{-3} at large distance, i.e. excatly of the same form as the effective hyperradial potentials. This should not be necessary if the proper components are accurately included. Instead this interaction should be of much shorter range in a three-body coordinate, e.g. exponential or Gaussian.

References

[1] E. Nielsen, D.V. Fedorov, A.S. Jensen and E. Garrido, The three-body problem with short-range interactions, Phys. Rep. **347** (2001) 373-459.

[2] A.S. Jensen, K. Riisager, D.V. Fedorov and E. Garrido, Structure and reactions of quantum halos, Rev. Mod. Phys. **76** (2004) 215-261.

[3] E. Garrido, D.V. Fedorov, A.S. Jensen and K. Riisager, Reaction mechanisms for two-neutron halo breakup, Phys. Rev. Lett. **86** (2001) 1986-1989.

[4] E. Garrido, D.V. Fedorov, A.S. Jensen and H.O.U. Fynbo, Anatomy of three-body decay:
I. Schematic models, Nucl. Phys. **A748** (2005) 27-38;
II. Decay mechanism and resonance structure, Nucl. Phys. **A748** (2005) 39-58;
III. Energy distributions, Nucl. Phys. **A 766** (2006) 74-96.

[5] E. Garrido, D.V. Fedorov and A.S. Jensen, Efimov effect in nuclear three-body resonance decays, Phys. Rev. Lett. **96** (2006) 112501(4).

[6] E. Garrido, D.V. Fedorov, H.O.U. Fynbo, and A.S. Jensen, Energy distributions of charged particles from three-body decay. Submitted for publication.

[7] E. Garrido, D.V. Fedorov and A.S. Jensen, Dipole excited states in ^{11}Li with complex coordinate rotation Nucl. Phys. **A 708** (2002) 277-299.

[8] B.V. Danilin, M.V. Zhukov, A.A. Korsheninnikov, L.V. Chulkov, V.D. Efros, Sov. J. Nucl. Phys. **46** (1987) 225.

[9] E. Garrido, D.V. Fedorov and A.S. Jensen, Comprehensive calculations of three-body breakup cross sections, Nucl. Phys. **A695**, 109-142 (2001).

[10] A.S. Jensen and K. Riisager, Towards necessary and sufficient conditions for halo occurrence, Phys. Lett. **B 480**, 39-44 (2000).

[11] K. Riisager, D.V. Fedorov and A.S. Jensen, Quantum halos, Europhysics Lett. **49** (2000) 547-553.

[12] A.S. Jensen, K. Riisager, D.V. Fedorov and E. Garrido, Classification of three-body quantum halos Europhysics Lett. **61** (2003) 320-326.

[13] A.S. Jensen and D.V. Fedorov, Efimov states in asymmetric systems Europhysics Lett. **62** (2003) 336-342.

[14] D.V. Fedorov, E. Garrido, and A.S. Jensen, Complex scaling of the hyper-spheric coordinates and Faddeev equations, Few-body systems, **33** (2003) 153-171.

[15] E. Garrido, D.V. Fedorov and A.S. Jensen, Origin of Borromean systems, Phys. Lett. **B 600**, 208-214 (2004).

[16] E. Garrido, D.V. Fedorov, and A.S. Jensen, Origin of three-body resonances, Eur. Phys. J. **A 25** (2005) 365-378.